A unified empirical model for quasielastic interactions of neutrino and antineutrino with nuclei

I. D. Kakorin*, kakorin@jinr.ru
K. S. Kuzmin*,**, kkuzmin@theor.jinr.ru
V. A. Naumov* vnaumov@theor.jinr.ru

* *Bogoliubov Laboratory of Theoretical Physics, Joint Institute for Nuclear Research, Joliot-Curie, 6, 141980, Dubna, Russia*
** *National Research Center "Kurchatov Institute" – A. I. Alikhanov Institute for Theoretical and Experimental Physics, B. Cheremushkinskaya, 25, 117218, Moscow, Russia*

Abstract

We propose a simple empirical model for evaluating the quasielastic neutrino- and antineutrino-nucleus cross sections, based on the conventional relativistic Fermi-gas model and the notion of running (dipole) axial-vector mass of the nucleon driven by two adjustable parameters (one of which is the ordinary axial mass of the nucleon). The suggested approach provides reasonable agreement with available consistent accelerator data on total, differential, and double differential quasielastic and quasielastic-like cross sections for different nuclear targets.

1 Introduction

An accurate calculation of the charged-current quasielastic (CCQE) neutrino-nucleus scattering cross sections remains an important issue to ensure the reliability and confidence level of extraction of neutrino oscillation parameters from atmospheric and accelerator neutrino experiments [1–15]. This problem is closely related to a large experimental uncertainty in the determination of the weak axial-vector and, to a lesser degree, pseudoscalar form factors of the nucleon and is reduced to the experimental uncertainty in the nucleon axial mass, M_A, which governs the Q^2 evolution of the axial form factor in the conventional dipole parametrization,

$$F_A\left(Q^2\right) = F_A(0)\left(1 + Q^2/M_A^2\right)^{-2},$$

where Q^2 is the modulus of the squared 4-momentum transfer (normalization of the form factor is chosen to be $F_A(0) = -1.267 \pm 0.003$).

Figure 1 provides a representative compilation of measurements of the dipole axial-vector mass: ANL 1969 [16], 1973 [17], 1975 [18], 1977 [19], 1982 [20]; BNL 1978 [21], 1980 [22], 1981 [23], 1988 [24], 1990 [25]; FNAL 1983 [26], 1984 [27, 28], 1987 [29]; MiniBooNE 2010 [30]; NOνA 2013 [31]; CERN SC 1968 [32]; HLBC 1966 [33], 1967 [34], [35], 1969 [36]; GGM 1977 [37], 1978 [38], 1979 [39,40]; BEBC 1990 [41]; NOMAD 2009 [42]; IHEP SKAT 1981 [43], 1988 [44], 1990 [45, 46]; IHEP–ITEP 1981 [47], 1982 [48], 1985 [49,50]; T2K ND280 2015 [51]. The values of M_A extracted from the flux-folded single-differential cross sections vs. Q^2, unnormalized Q^2-distributions, flux-folded double-differential cross sections, and total CCQE cross sections are shown by, respectively, squares, circles, lower triangles, and upper triangles. Filled and open symbols denote the analyses of rates and shapes, respectively. The data are grouped by nuclear targets. The figure shows a wide scatter of data points. Partly this is because the data of different experiments were obtained using rather different input parameters, models for the nuclear effects and final-state interactions (FSI), electromagnetic form factors, etc.,[1] but the observed discrepancies sometimes exceed the expected systematic errors. The solid vertical lines represent the best fit value of

[1] In some cases the result is dependent on extraction methods and data subsets used in the analyses; for example, in the recent T2K analyses [51], the effective M_A parameter was measured to be $1.26^{+0.21}_{-0.18}$ GeV or $1.43^{+0.28}_{-0.22}$ GeV by using, respectively, the absolute or shape-only $p_\mu - \cos\theta_\mu$ event distributions. In Fig. 2 we show the first value only.

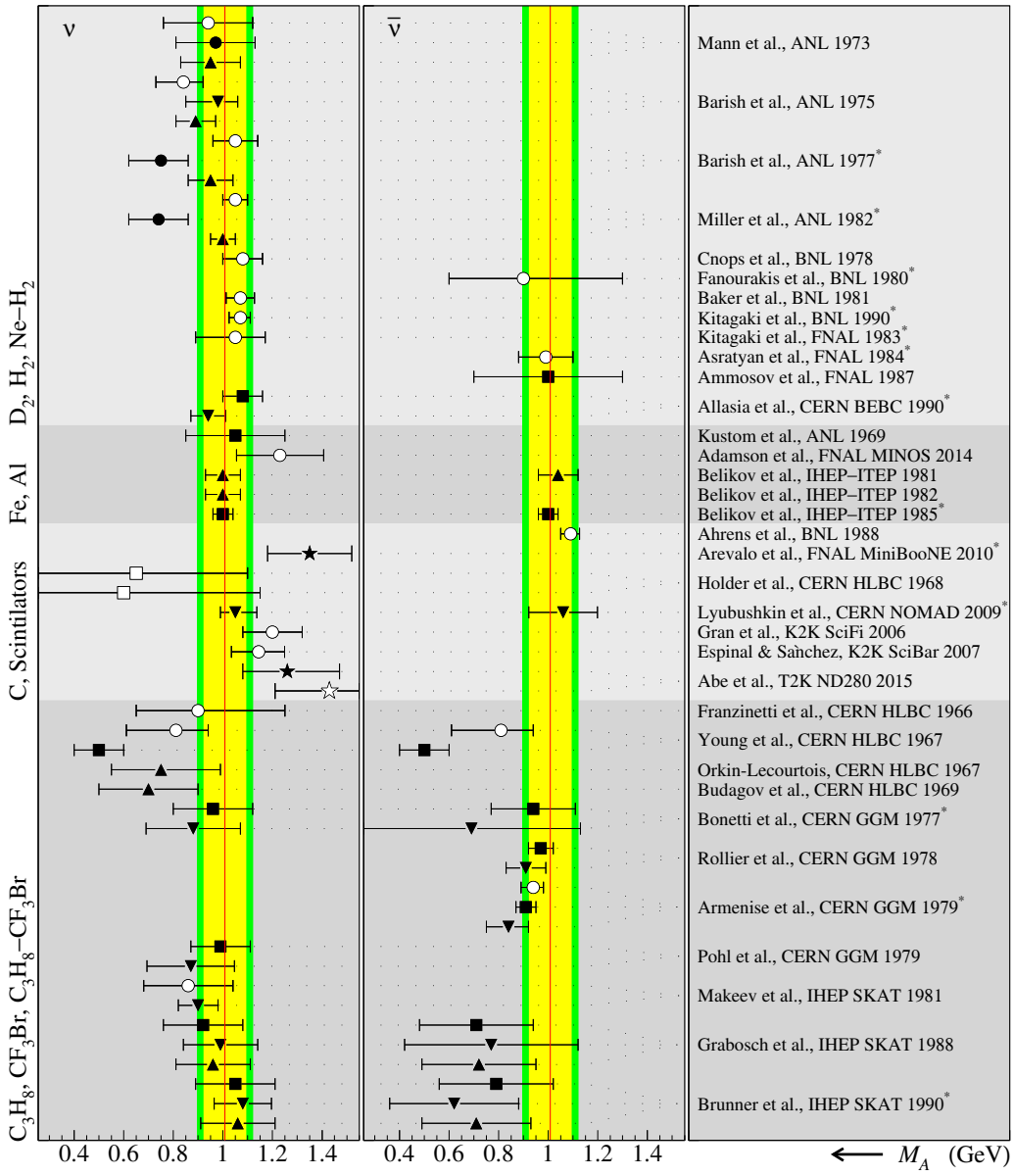

Figure 1: A summary of the nucleon axial-vector mass measurements in experiments with different nuclear targets (see main text for explanations).

M_A obtained in the particular part of our statistical analysis, based on the "golden" (i.e., consistent and non-overlapping) data of the experiments with

deuterium and hydrogen targets (see below, section 3). Shaded confidence bands around the lines represent 1σ and 2σ deviations from the best-fitted values of M_A and, in this instance, provide a "framework" for comparison of the data. We can in particularly conclude that there is no statistically significant indication of correlations between the observed data scatter and nuclear targets.

Several efforts were made in recent years to safely extract the value of the parameter M_A from ν_μD, $\overline{\nu}_\mu$H, and $\pi^\pm$ electroproduction experiments [52–55], and also from all available at that time data on $\nu/\overline{\nu}$ scattering off hydrogen, deuterium, and heavier nuclei [56–58]. In the latter studies, the nuclear effects were accounted for by using the closure over the dinucleon states and one-pion exchange currents [59–61] for deuterium targets, and by applying the Smith-Moniz relativistic Fermi-gas (RFG) model [62] (implemented in many Monte Carlo neutrino event generators) for heavier nuclear targets. The most accurate models for the nucleon electromagnetic form factors were used in these calculations. It has been inferred from these studies that the most of the then-existing $\nu_\mu/\overline{\nu}_\mu$ CCQE and pion electroproduction data could be satisfactorily described with $M_A \simeq 1$ GeV to within a few percent accuracy (cf. lines in Fig. 1). This conclusion was reached before the modern high-statistics measurements of the $\nu_\mu/\overline{\nu}_\mu$ CCQE scattering from carbonaceous targets, performed in the FNAL experiments MiniBooNE [30, 63], SciBooNE [64,65], MINERνA [66–68], and MINOS [69], and also in the T2K experiments with the near detectors ND280 (off-axis) [51, 70–73] and INGRID (on-axis) [74]. According to our RFG-based calculations, the MiniBooNE CCQE double-differential cross section data [30, 63] are well described with $M_A = 1.36 \pm 0.06$ and 1.31 ± 0.03 GeV for, respectively, ν_μ and $\overline{\nu}_\mu$ beams (cf. also [75]). These values are in reasonable agreement with other recent low-energy data but are not compatible with the values of 1.07 ± 0.11 GeV (ν_μ) and 1.08 ± 0.19 GeV ($\overline{\nu}_\mu$), extracted from the data obtained at higher energies by the NOMAD experiment [42] as well as with the results of the above-mentioned analyses [52–58].

Figure 2 shows the effective values of $M_A = M_A^{\rm RFG}$ obtained (by using the standard RFG model) in several recent experiments [30, 42, 69, 74, 76, 77] with composite (mainly carbon-rich) nuclear targets; the data are plotted as a function of the mean energy of the $\nu_\mu/\overline{\nu}_\mu$ beams. The dashed straight line with the shaded double band has the same meaning as the straight lines with bands in Fig. 1; that is, it represents the result of our statistical analysis of the "golden" data. It is evident that the values of M_A extracted from the

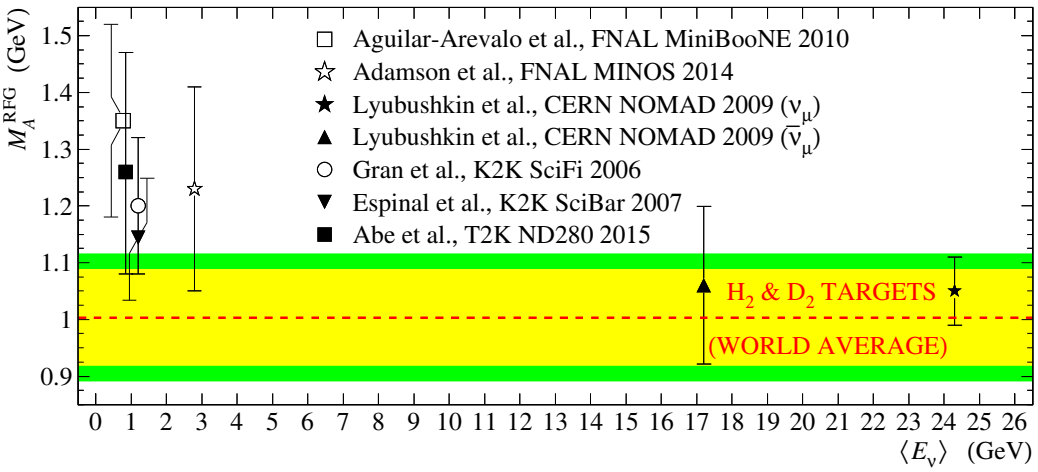

Figure 2: The nucleon axial mass values vs. mean $\nu_\mu/\overline{\nu}_\mu$ beam energy, obtained in the experiments MiniBooNE [30], MINOS [69], NOMAD [42], K2K SciFi [76], K2K SciBar [77], and T2K ND280 [51] within the standard RFG model. The dashed straight line and surrounding shaded double band represent the M_A value and its 1σ and 2σ uncertainties, as extracted from available deuterium data.

low-energy data on heavy nuclear targets are in conflict with the deuterium data and also with the higher-energy NOMAD data. Moreover – and this is the key observation – the data provide a hint that M_A increases with decreasing the mean $\nu_\mu/\overline{\nu}_\mu$ energy. Empirically, this is simply a *repercussion* of the observed growth of the total CCQE cross sections in nuclear matter at low energies.

Contemporary explanations of this growth include the effects beyond the scope of the naive RFG approach and impulse approximation (IA). Among these are several RFG extensions, such as local Fermi gas (LFG) model [78], local density approximation (LDA) [79], and spectral function (SF) approach [80–85]; relativistic mean field and relativistic Green's function models [86,87]; meson-exchange currents (MEC), intermediate Δ isobar or multi-nucleon excitations [11, 88], short-range and long-range correlations within random phase approximation (see, e.g., refs. [89–91]); a phenomenological $2p-2h$ MEC solution is also included into the GiBUU model [92, 93] based on quantum-kinetic transport equations; parametrization of the observed enhancement in the transverse electron quasielastic response function (presumably because of MEC) [94,95]; a variety of so-called superscaling models, e.g.,

SuSA [96], SuSAv2 [97], SuSAv2-MEC [98–100], and SuSAM* [101,102]. The most comprehensive microscopic or phenomenological models provide better data explanation without increasing M_A (see refs. [103–108] for reviews and further references).

The aims of this paper are to clarify the experiential state-of-the-art with the nucleon axial mass and provide a simple phenomenological "recipe" for an accurate description of the CCQE ν and $\overline{\nu}$ interactions with nuclei at energies of interest for neutrino oscillation experiments, within the frameworks of conventional RFG model, but at the expense of having two adjustable parameters (instead of one, M_A) in the nuclear axial-vector structure function. The suggested recipe can easily be implemented in the Monte Carlo event generators[2] being used in the analyses of the experiments with accelerator and atmospheric $\nu/\overline{\nu}$ fluxes.

2 Running axial mass

The idea of the proposed method is to calculate the cross sections for the CCQE $\nu/\overline{\nu}$ interactions with nuclei other than hydrogen and deuterium by using in the charged weak hadronic current the neutrino energy dependent *running* axial-vector mass, $M_A^{\rm run}(E_\nu)$, in place of the conventional constant axial-vector (dipole) mass M_A, and the latter will be referred to as the *current* or *conventional* axial mass. The lab-frame neutrino energy, E_ν, is treated as Lorentz invariant, $E_\nu = (s - M^2)/2M$, where M is the mass of the target nucleus, and IA is assumed. With such a customization, the modified hadronic current retains its Lorentz-transformation property albeit loses the fundamental meaning; it is no longer a function of Q^2 only and thus it can be employed only as an *artificial prescription* to account for the *energy-dependent* nuclear effects beyond RFG and IA.

In so doing, the specific energy dependence of $M_A^{\rm run}$ is determined from the available robust experimental data on the CCQE interactions. The function of energy, $M_A^{\rm run}(E_\nu)$, will be in general different for different modifications of the RFG models and other input parameters, but in any case this function must be parametrized in such a way that it asymptotically approaches the current axial mass value at high energies and well describes the lower-energy

[2]It is already implemented into the GENIE neutrino generator (version 2.11.0 and higher) as an option.

data. In the present analysis we adopt the following very simple parametrization,

$$M_A^{\rm run} = M_0 \left(1 + \frac{E_0}{E_\nu}\right), \tag{1}$$

in which the constant parameters M_0 and E_0 are obtained from a global fit to available accelerator data on the ν_μ and $\overline{\nu}_\mu$ CCQE interactions with nuclei. It turns out that the parametrization (1) is universal in the sense that it works rather well for all medium to heavy nuclear targets and at all accessible $\nu/\overline{\nu}$ energies.

In our fit to $M_A^{\rm run}$, the ν_μD and $\overline{\nu}_\mu$H cross sections are used for adjusting the parameter M_0 only, inasmuch as the $M_A^{\rm run}(E_\nu)$ can be applied to the $\nu/\overline{\nu}$ CCQE scattering from the heavier nuclear targets. Since $M_A^{\rm run} \to M_0$ at high energies, $E_\nu \gg E_0$, where the RFG approach works rather well, the constant M_0 can be treated as the current axial-vector mass M_A. On the other hand, the value of M_A can be independently extracted from a fit to the ν_μD data for which the nontrivial (beyond RFG) nuclear effects are relatively small and better understood.

The nuclear Fermi momenta, p_F, and binding energies (usually identified with the separation energies), E_b, are rather uncertain and values of these parameters used in the literature vary widely.[3] For a unification, in the subsequent calculations we use the following interpolation formulas:

$$p_F = 270\left[1 - 4.2/A + (6.0/A)^2 - (5.3/A)^3\right]\ \text{MeV},$$
$$E_b = 50.4\left[1 - 2.26/\xi + (1.73/\xi)^2 - (1.21/\xi)^3\right]\ \text{MeV}.$$

Here $\zeta = Z/A^{1/3}$. These interpolations are obtained from all available data on electron-nucleus scattering [110, 111] and are sufficiently accurate for all nuclei with $A \geq 6$. The proton and neutron Fermi momenta are calculated in the conventional way [112] as, respectively, $p_F^p = (2Z/A)^{1/3} p_F$ and $p_F^n = (2N/A)^{1/3} p_F$, where $N = A - Z$. These relations are based on the simplest assumption that the density of nuclear matter is approximately constant irrespective of the proton-to-neutron ratio Z/N.

Other ingredients of the standard formalism of the CCQE $\nu/\overline{\nu}$ scattering on nucleons and nuclei are described in detail in [58], all input parameters are updated according to the recent review [113].

[3] See [109] for a more sophisticated treatment of these matters.

3 Statistical analysis

The measurements of the CCQE $\nu_\mu/\overline{\nu}_\mu$ cross sections were carried out from the mid-60s to present day, in the experiments at ANL [16–20, 114–117]; BNL [21–25,118,119]; FNAL [26–31,63–67,120]; LANL (LSND) [121], CERN [32–37,39–42,122–128]; IHEP [43–45,47–50,129]; K2K [76]; and T2K [51,70–72, 74]. The detector targets used in these experiments are hydrogen [22], deuterium [17–21,23,25,41,115–117,119], water [76], mineral oil [30,63,66,67], aluminium [47–50], argon [128], iron [31, 120], steel [16], carbon-rich (e.g., hydrocarbonic, like propane or polystyrene) targets [24, 32, 36, 42, 64, 65, 118, 121], freon [18,26,33–35,37,43–45,122–126,129], propane–freon mixtures [39, 40, 126, 127], neon–hydrogen mixtures [27–29], and complex carbonaceous targets of the T2K near detectors [51,70–72,74]. In many cases, the detector targets contain small amounts of other materials and impurities, all of which are taken into account in our calculations.

For the statistical analysis, we use the data on the total (σ), flux-averaged single-differential ($\langle d\sigma/dQ^2\rangle$), and double-differential ($\langle d^2\sigma/dE_\mu d\cos\theta_\mu\rangle$) cross sections, as well as the flux-weighted or measured at the mean $\nu_\mu/\overline{\nu}_\mu$ energy Q^2-distributions ($\langle dN/dQ^2\rangle$ or dN/dQ^2). The full dataset is formed by the results of the self-contained measurements satisfying the selection criteria described in [58]. Namely, we use the results of the following experiments:

- Hydrogen: BNL 1980 [22] ($dN_{\overline{\nu}}/dQ^2$, 5);
- Deuterium: ANL 1977 [19] (σ_ν, 8), ANL 1982 [20] ($\langle dN_\nu/dQ^2\rangle$, 39), BNL 1990 [25,119] ($\langle dN_\nu/dQ^2\rangle$, 37), FNAL 1983 [26] ($\langle dN_\nu/dQ^2\rangle$, 20), and CERN BEBC 1990 [41] ($\langle d\sigma_\nu/dQ^2\rangle$, 8);
- Neon-Hydrogen mixture: FNAL 1984 [27, 28] ($dN_{\overline{\nu}}/dQ^2$, 14);
- Aluminium: IHEP–ITEP 1985 [49, 50] (σ_ν, $\sigma_{\overline{\nu}}$, $\langle d\sigma_{\nu+\overline{\nu}}/dQ^2\rangle$, 8 in each set);
- Carbon-rich targets: CERN NOMAD 2009 [42] (σ_ν, $\sigma_{\overline{\nu}}$, 10 and 6, respectively), FNAL MiniBooNE 2010 [30] ($\langle d^2\sigma_\nu/dE_\mu d\cos\theta_\mu\rangle$, 137), FNAL MiniBooNE 2013 [63] ($\langle d^2\sigma_{\overline{\nu}}/dE_\mu d\cos\theta_\mu\rangle$, 78);
- Freon, Propane, & their compounds: CERN GGM 1979 [39,127] ($\langle dN_{\overline{\nu}}/dQ^2\rangle$, 13), LAr-TPC 2007 [128] (σ_ν, 1) and IHEP SKAT 1990 [45] ($\langle d\sigma_\nu/dQ^2\rangle$,

$\langle d\sigma_{\overline{\nu}}/dQ^2\rangle$, 8 and 7, respectively), T2K INGRID 2015 [74] (σ_ν, 2) and T2K ND280 2015 [51] (σ_ν, 5).

In the brackets we show the data types and numbers of experimental bins involved into the statistical analysis. Thus the full dataset consists of 422 bins with 290, 124, and 8 bins for, respectively, ν_μ (68.7% of the full dataset), $\overline{\nu}_\mu$ (29.3%), and cumulative $\nu_\mu + \overline{\nu}_\mu$ (1.9%) subsets. The full dataset represents 215, 31, 128, and 48 bins for, respectively, the flux-folded double differential cross sections measured by MiniBooNE (51% of the full dataset), single-differential in Q^2 cross sections (7.4%), unnormalized Q^2-distributions (30.3%), and flux-unfolded total cross sections (11.4%). The dataset used for extraction of the current axial mass M_A ($\equiv M_A^{\rm D}$) contains 117 bins (27.7% of the full dataset) and is formed by the results of ANL 1977 [19], 1982 [20], BNL 1980 [22], 1990 [25,119], FNAL 1983 [26], and CERN BEBC 1990 [41]. We do not utilize the results of several modern experiments as MINERνA [66–68, 130–133], MiniBooNE [134], and T2K [72, 73, 135]. Instead, we use the modern data for a verification of our model (see next section).

The analysis is based on the standard least-square statistical model:

$$\chi^2 = \sum_i \left\{ \sum_{j\in G_i} \frac{\left[N_i T_{ij}(\boldsymbol{\lambda}) - E_{ij}\right]^2}{\sigma_{ij}^2} + \frac{\left(N_i - 1\right)^2}{\sigma_i^2} \right\}. \qquad (2)$$

Here the index i enumerates the experiments (or data groups) G_i, index $j \in G_i$ enumerates the bin-averaged experimental data E_{ij} from the group G_i, σ_{ij} is the error of E_{ij}, without the uncertainty due to the overall normalization. The normalization factor, N_i (individual for each data group G_i), is treated as fitting parameter and included into the ordinary penalty term, $\left(N_i - 1\right)^2/\sigma_i^2$, where σ_i is the normalization error. The value $T_{ij}(\boldsymbol{\lambda})$ represents the associated (also bin-averaged) model prediction, dependent on the set of fitting parameters $\boldsymbol{\lambda}$; in our particular two-parameter case, $\boldsymbol{\lambda} = M_0$ for hydrogen and deuterium targets and $\boldsymbol{\lambda} = (M_0, E_0)$ for all other nuclear targets. The minimization procedure can be significantly simplified by substituting into Eq. (2) $N_i = \mathcal{N}_i(\boldsymbol{\lambda})$, where the functions $\mathcal{N}_i(\boldsymbol{\lambda})$ are obtained from the analytic solution to the equations $\partial\chi^2/\partial N_i = 0$,

$$\mathcal{N}_i(\boldsymbol{\lambda}) = \frac{1 + \sigma_i^2 \sum_{j\in G_i} \sigma_{ij}^{-2} T_{ij}(\boldsymbol{\lambda}) E_{ij}}{1 + \sigma_i^2 \sum_{j\in G_i} \sigma_{ij}^{-2} T_{ij}^2(\boldsymbol{\lambda})}.$$

The χ^2 for the final fit to all data includes an additional penalty term

$$\left[\left(M_0 - M_A^{\rm D}\right)/\Delta M_A^{\rm D}\right]^2,$$

which provides a "soft anchoring" of the parameter M_0 to the current axial mass value, $M_A^{\rm D} \pm \Delta M_A^{\rm D}$, obtained by fitting the robust ("golden") deuterium data only.

For extracting the value of M_A from the CCQE ν_μD data, the authors of the experiments (see, e.g., refs. [23,25,26]) usually take into account the Pauli exclusion principle, Fermi motion, and deuteron binding by using the correction factor derived in refs. [59, 60]. In our analysis we use (when available) the raw, uncorrected ν_μD data (mainly Q^2-distributions). To account for the nuclear effects in the ν_μD interactions, we adopt the closure approximation over the dinucleon states following [61], where the MEC contributions were estimated using single-pion exchange diagrams in the static limit. In our calculations, the Reid hard-core potential and Hulthen wave function for the deuteron are adopted, as providing the best description of the ν_μD data.

All the fits are done with the CERN function minimization and error analysis package MINUIT [136, 137]. The errors of the output parameters quoted below correspond to one and two standard deviation. As follows from the analysis, the deviation of the normalization factors N_i from unity for each data group G_i does not exceed the doubled experimental uncertainty of the corresponding data normalization; in most cases these factors are very close to unity.

As a result of the analysis, the best-fit value of $M_A^{\rm D}$ is found to be

$$M_A^{\rm D} = 1.003^{+0.083\,(0.109)}_{-0.083\,(0.108)}\ \text{GeV} \tag{3}$$

with the corresponding χ^2/ndf value to be $127.5/(117-7) \approx 1.16$. The best-fit values of the running axial mass parameters are found as follows:

$$M_0 = 1.052^{+0.095\,(0.114)}_{-0.094\,(0.113)}\ \text{GeV}, \quad E_0 = 278^{+130\,(158)}_{-111\,(131)}\ \text{MeV}, \tag{4}$$

with $\chi^2/\text{ndf} = 272.7/(422-19) \approx 0.68$.

As the next step, by taking into account that the RFG calculations well describe the high-energy data on all nuclear targets with the unique value of M_A ($\approx M_A^{\rm D} \approx 1$ GeV) [58], we add to the sum (2) the penalty term $\left(M_0 - 1.003\right)^2/0.083^2$ to constrain the bias of M_0 from the deuterium axial

mass $M_A^{\rm D}$ (3). The final global fit performed using this constraint ("soft anchoring") yields

$$M_0 = 1.008 \pm 0.025\,(0.029)\ \text{GeV}, \quad E_0 = 331^{+57\,(69)}_{-54\,(64)}\ \text{MeV} \tag{5}$$

with $\chi^2/\text{ndf} = 277.6/(422-19) \approx 0.69$. The obtained value of M_0 is in very good agreement with (3) and with the results of earlier extractions of the current axial mass [52–58].

Figure 3 shows that the best-fit values of the parameters obtained in the

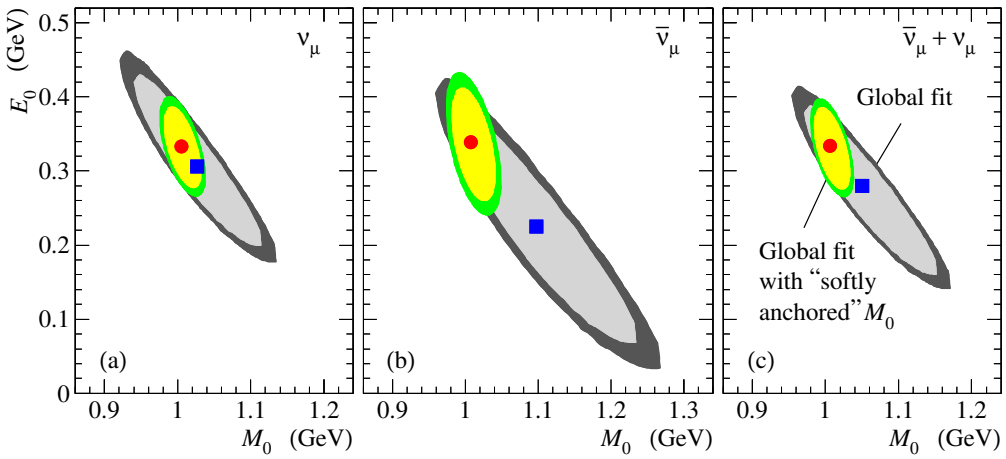

Figure 3: Error contours for the parameters M_0 and E_0 obtained in the global statistical analyses of the ν_μ (a), $\overline{\nu}_\mu$ (b), and $\nu_\mu + \overline{\nu}_\mu$ (c) CCQE data subsets. Circles and squares represent the best-fit points (M_0, E_0) obtained from the global fits performed with and without "soft anchoring" of the parameter M_0 (by adding the related penalty term to the χ^2 sum) and given by (4) and (5), respectively. The inner and outer contours for both these fits indicate, respectively, the 68% and 95% C.L. confidence regions.

separate analyses of the $\nu_\mu + \overline{\nu}_\mu$, ν_μ or $\overline{\nu}_\mu$ data are in agreement with each other within the corresponding 1σ confidence contours. In the antineutrino case (where the dataset is more fragmentary than that for neutrino) the agreement is worse but still acceptable.

It should be noted that in the strict sense the obtained values of $M_A^{\rm D}$ and of the parameters M_0 and E_0 are only valid for the "BBBA$_{25}$(07)" model of the vector form factors of the nucleon [54]. However, as follows from our examinations, these parameters are not very responsive to variations of the

vector form factors within reasonable limits. In other words, one can use (while with caution) the obtained values of $M_A^{\rm D}$, M_0, and E_0 also together with models other than BBBA$_{25}$(07) as well as with some modifications of the RFG approach (e.g., LFG [78] or Bodek–Ritchie RFG [138]).

As a qualitative test of self-consistency of our approach, we collect in Fig. 4 a representative set of the current axial mass values extracted, within the SM RFG model with the unified set of inputs, from the individual fits of the data subsets involved in the global analysis. The M_A values are plotted in function of the mean (anti)neutrino energy of interaction defined as

$$\langle E_\nu \rangle_{\rm int} = \frac{\int E_\nu F_\nu(E_\nu) \sigma_{\rm tot}^{\rm CCQE}(E_\nu) dE_\nu}{\int F_\nu(E_\nu) \sigma_{\rm tot}^{\rm CCQE}(E_\nu) dE_\nu}, \tag{6}$$

where $F_\nu(E_\nu)$ is the (anti)neutrino energy spectrum in the related experiment and $\sigma_{\rm tot}^{\rm CCQE}(E_\nu)$ is the total CCQE cross section for the detector target used in the experiment. Although this quantity is moderately model-dependent, it is a bit more appropriate for the verification than the mean (anti)neutrino beam energy, $\langle E_\nu \rangle$, used in Fig. 2. The points represent the values of M_A derived from the formal fits (separately for each experiment) to the CCQE data obtained with the following nuclear targets:

- Deuterium: ANL 1977 [19] (0.90 GeV), ANL 1982 [20] (0.90 GeV), BNL 1990 [25, 119] (1.47 GeV), FNAL 1983 [26] (23.5 GeV), CERN BEBC 1990 [41] (53.5 GeV);
- Neon-Hydrogen mixture: FNAL 1984 [27] (7.3, 13.6, and 26.4 GeV);
- Carbonaceous targets: FNAL MiniBooNE 2010 [30] (0.93 GeV), FNAL MiniBooNE 2013 [63] (0.90 GeV), FNAL MINERνA 2013 [66,67] (3.5 GeV for ν_μ and 3.4 GeV for $\overline{\nu}_\mu$), CERN NOMAD 2009 [42] (23.8 GeV for ν_μ and 19.3 GeV for $\overline{\nu}_\mu$), T2K ND280 2015 [51] (0.948 GeV), T2K INGRID 2015 [74] (0.950 GeV);
- Freon: IHEP SKAT 1990 [45] (6.4 GeV for ν_μ and 6.0 GeV for $\overline{\nu}_\mu$);
- Propane-Freon mixture: CERN GGM 1979 [39, 127] (2.4 GeV);
- Argon: CERN LAr-TPC 2007 [128] (23.8 GeV);
- Aluminum: IHEP–ITEP 1985 [49] (5.7 GeV – the mean for ν_μ and $\overline{\nu}_\mu$);

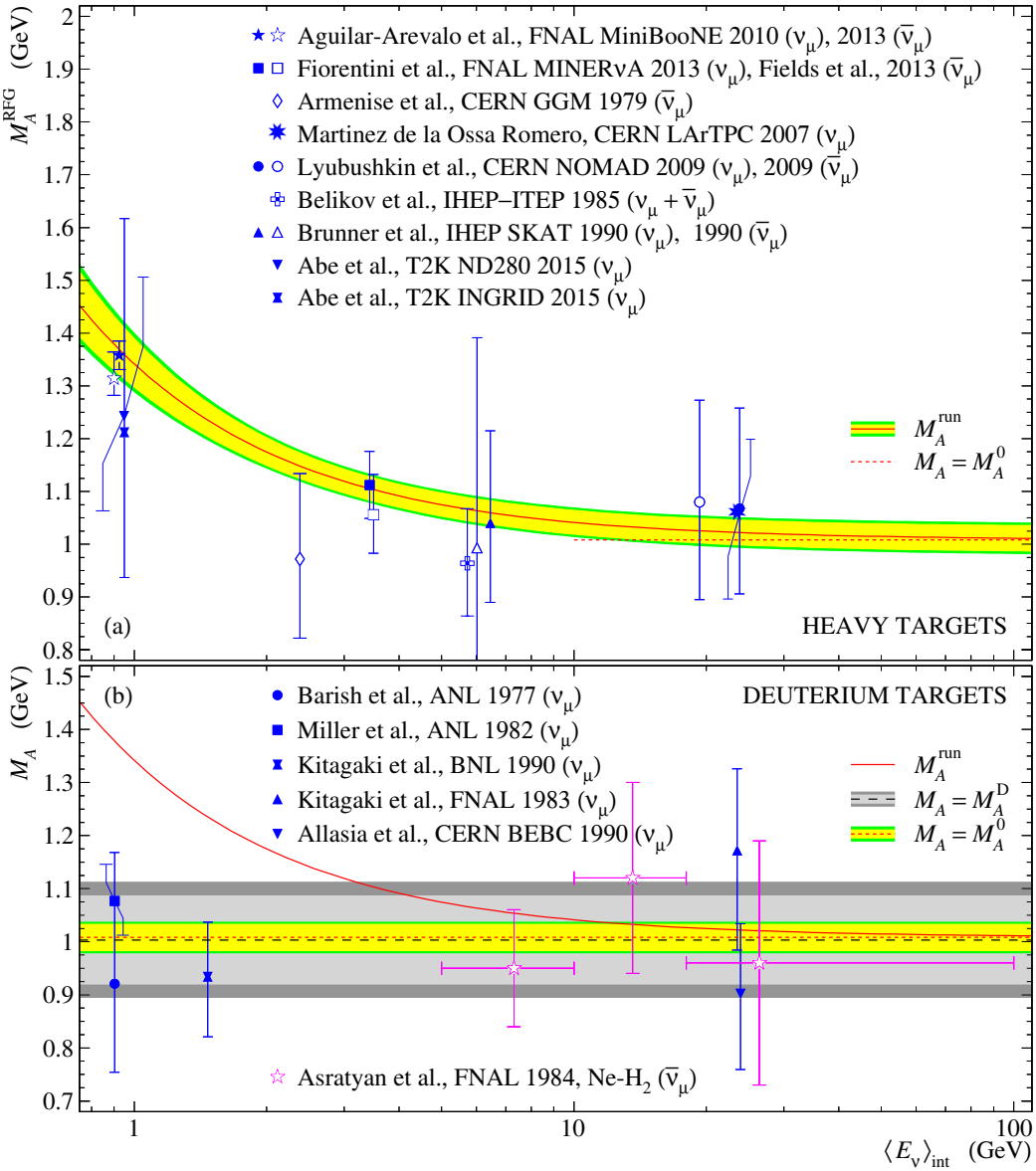

Figure 4: The current axial mass extracted from different experiments and plotted vs. the mean energy of interaction (see main text for explanations).

- Iron: T2K INGRID 2015 [74] (0.95 GeV).

The numbers in brackets in the above list represent the values of $\langle E_\nu \rangle_{\rm int}$ estimated from eq. (6) by using the relevant ν_μ and $\overline{\nu}_\mu$ energy spectra and

the CCQE cross sections calculated with the constant $M_A = M_0$ for the deuterium data[4] and with the running axial mass (with the parameters extracted from the global fit) for all other data, except for the FNAL 1984 experiment [27], where author's extractions of M_A for the three energy ranges are shown (for the energy binning definition used in [27], the differences between $\langle E_\nu \rangle_{\rm int}$ and $\langle E_\nu \rangle$ is unimportant). The solid curves represent the energy dependence of $M_A^{\rm run}$ on the parameters (5) and the straight dashed and dotted lines show the cases $M_A = M_A^{\rm D}$ and $M_A = M_0$, respectively. The filled double bands show the 1σ and 2σ confidence regions due to uncertainties in the parameters of $M_A^{\rm run}$ (top panel) and $M_A^{\rm D}$ and M_0 (bottom panel). It is clearly seen that the deuterium data are consistent with constant M_A while the data for heavier nuclei correlate with the energy dependent (running) axial mass. The result of [27] is formally consistent with both constant and running M_A but the former is statistically more preferable. Similar extractions of M_A as a function of energy were performed earlier, in the neutrino experiments at BNL [23] and FNAL [26] with deuterium filled bubble chambers. Both experiments obtained no significant variation of M_A with energy and are in agreement with our result (3). And lastly, there is no statistically significant difference between the energy dependencies of M_A obtained in the studies of neutrino and antineutrino interactions with heavier than deuterium nuclei.

4 Comparison with the recent data

To test our model, we compare the calculations with predictions of several other modern models and with selected recent data on the total (Fig. 5) and double-differential (Figs. 6— 12) cross sections of the on ν_μ and $\overline{\nu}_\mu$ CCQE and CCQE-like interactions with nuclei. We emphasize that the data displayed in these figures by open symbols have not been involved into the global statistical analysis described above.

All calculations are performed using the GENIE 3 MC generator [140]. To simulate the CCQE-like interactions we apply two incorporated FSI models called hA 2018 and hN 2018. The hA 2018 model evaluates the probabilities of emission, absorption, and recharge of nucleons and light mesons with kinetic energies up to 1.2 GeV by using available heuristic data on relevant cross sec-

[4]Recall that the ν_μD cross sections are calculated using the Singh-Arenhovel model [61]. The estimated values of $\langle E_\nu \rangle_{\rm int}$ are almost insensitive to variations of M_0 within 2σ uncertainty.

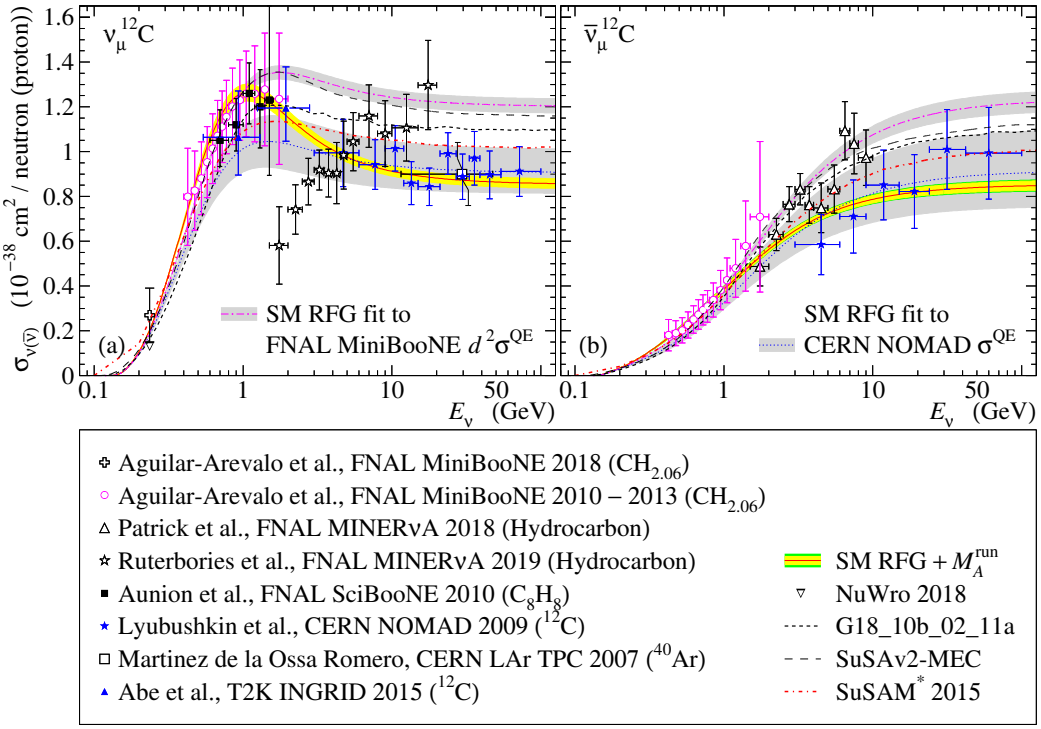

Figure 5: Total CCQE ν_μ (a) and $\overline{\nu}_\mu$ (b) cross sections per interacting nucleon as measured in MiniBooNE [30, 63, 134], SciBooNE [64, 65], LAr-TPC [128], NOMAD [42], T2K INGRID [74], and MINERνA [132, 139] (not a true total cross sections, but rather differential cross sections vs. $E_\nu^{\rm QE}$ extracted by applying several kinematic cuts, see text). The vertical error bars represent the total experimental errors including the $\nu_\mu/\overline{\nu}_\mu$ flux normalization uncertainties. The data points marked with open symbols were not included into the statistical analysis. The solid curves and narrow inner/outer bands correspond to the best-fit values of M_0 and E_0 (5) and $1\sigma/2\sigma$ deviations from the best fit. The dashed-dotted and dotted curves represent, respectively, the SM RFG predictions with the values of the axial mass, $M_A^{\rm RFG}$, obtained by two-parameter fits to the MiniBooNE double-differential CCQE cross section dataset ($CH_{2.06}$) and the NOMAD CCQE dataset on $\sigma_{\rm tot}^{\rm QE}$ (pure carbon), performed separately for neutrinos and antineutrinos. The gray bands show the 1σ uncertainty due to the fitting errors of $M_A^{\rm RFG}$ and normalization factors. The other curves show predictions of GENIE 3 tune G18_10b_02_11a, SuSAv2-MEC, and SuSAM*. Also shown the NuWro generator prediction for the neutrino cross section at $E_\nu = 236$ MeV.

tions for the atomic nuclei from helium to lead. The isospin symmetry is used to recalculate the cross sections for neutral pions from the charged pion data. At energies above 300 MeV, the phenomenological cascade-exciton model CEM03 [141–143] is applied. The cascade is simulated for an iron nucleus and the cross sections for other nuclei are obtained simply by a re-scaling with the factor $\propto A^{2/3}$. The pion absorption is decomposed into two simulation branches: the two-nucleons and multi-nucleon absorption; the split probability is defined from empirical data. Multiple final-state hadrons are distributed in the phase space. The hN 2018 model simulates reactions of all types for any target nucleus. It uses partial wave analysis of available data on the πN, KN, and NN cross sections as provided by the Scattering Analysis Interactive Dial-in (SAID) program [144–146]. For pions with kinetic energy below 350 MeV the model uses the method of [147] which combines a microscopic calculation of the intrinsic probabilities for each reaction channels and a simulation procedure for the pion transport. The pion absorption is simulated on separate nucleons. The hN 2018 model can simulate pre-equilibrium and compound nuclear states. The simulations of hadron transport through a nuclear medium have some common features in the hA 2018 and hN 2018 models.

In all calculations with the SM RFG + $M_A^{\rm run}$ model we employ several modification of the default GENIE 3 configuration. In particular, for estimation of the single-pion production (one of the most important contribution to post-FSI CCQE-like) we use the extended Rein-Sehgal model (ExRS) [148, 149] supplemented by the pion-pole contribution to the hadronic axial current [150]. Instead of the GENIE default "resonance" axial mass value $M_A^{\rm RES} = 1.12$ GeV [57], we use the updated value of 1.18 GeV which we obtained from a new global fit to the ν_μD single-pion production data. The input parameters (resonance masses and widths, decay fractions) are updated according to the most recent data [113]. Pauli blocking is added into all GENIE 3 resonance pion production models. Next, we refused the default renormalization of the Breit-Wigner factors. Among several physical and technical reasons, we only mention here that the normalization integral for the S-wave resonances diverges, leading to an unreasonable ambiguity due to an unphysical cutoff in invariant hadronic mass. The simplest way to avoid this ambiguity is to rule out the renormalization at all. It should be remarked that the GENIE 2 default parametrization of the vector CCQE form factors, the BBA(05) model [151], has been replaced in GENIE 3 to a more accurate $\rm BBBA_{25}(07)$ model [54].

Figure 5 shows the total ν_μ and $\overline{\nu}_\mu$ CCQE cross sections measured in the experiments NOMAD [42] (carbon-rich target with $\langle Z\rangle/\langle A\rangle \simeq 0.524$), SciBooNE [64, 65] (polystyrene), MiniBooNE [30, 63, 134] (mineral oil), and T2K ND280 [51] (carbon); all these data are converted to pure carbon. Also shown the unconverted data from LAr-TPC [128] (argon),[5] and very recent MINERνA measurements [132, 139] (hydrocarbon with admixtures, $\langle Z\rangle/\langle A\rangle \simeq 0.54$). The latter data fill the gap between the MiniBooNE and NOMAD data. However the MINERνA data are obtained using several restrictions on the lepton and final nucleon observables (the main of which is the cut in the muon scattering angle $\theta_\mu < 20^\circ$) that makes difficult a direct quantitative comparison with other data shown in Fig. 5. These kinematic cuts are not very essential in the high-energy region but considerably reduce the cross sections at energies below 5–6 GeV. A quantification of the effect is model dependent; according to our model estimations, there is no actual conflict between the MINERνA and MiniBooNE results for both neutrino and antineutrino datasets, but the tension between the neutrino data of MINERνA and NOMAD is even larger than is seen in the figure. Another difficulty for a direct comparison of the data is due to the complex chemical composition of the MINERνA detector medium. A conversion of the MINERνA data to uncombined carbon (also model-dependent) only enhances the discrepancy between the NOMAD and MINERνA for neutrinos but partially eliminates it for antineutrinos, making the tension softer.

Taking into account the foregoing, we can conclude that the SM RFG + $M_A^{\rm run}$ model is in quite good agreement with all the data in Fig. 5 except for the MINERνA ν_μ [139] and (to a lesser extent) $\overline{\nu}_\mu$ [132] cross sections which, in turn, – let us repeat – conflict with the NOMAD data [42].

For contrasting purposes, we also show calculations made with the best-fit values of effective $M_A^{\rm RFG}$ extracted within the standard SM RFG model separately from the MiniBooNE double-differential cross sections ($M_A^{\rm RFG} = 1.36\pm0.06$ GeV for ν_μ and 1.31 ± 0.03 GeV for $\overline{\nu}_\mu$) and from the NOMAD total CCQE cross sections ($M_A^{\rm RFG} = 1.07 \pm 0.11$ GeV for ν_μ and 1.08 ± 0.19 GeV for $\overline{\nu}_\mu$).[6] In Fig. 5 we also display the predictions of four other models.

[5] The expected difference between the cross sections (per neutron) on argon and carbon is fully negligible at energies under consideration.

[6] To minimize the total uncertainty, we use the data for the real MINERνA and NOMAD targets and do not use those converted to carbon. We mention in passing that our estimations of $M_A^{\rm RFG}$ somewhat different from those reported by the experimenters since we use different input parameters and models for the vector form factors.

Calculation at the point $E_\nu = 236$ MeV (borrowed from [134]) is based on an updated version of the NuWro MC neutrino event generator [152]. The GENIE tune G18_10b_02_11a (one of the most comprehensive physics tunes incorporated in GENIE 3, based on the model by Nieves et al. [153] and adjusted to the current data) does not contradict to the low-energy data and fits the higher energy part of the MINERνA result rather than that of NOMAD. The SuSAv2-MEC model [98] works very well at low energies and predicts even larger high-energy cross sections than G18_10b_02_11a. The prediction of another superscaling model, SuSAM* [101], manages to squeeze between Scylla and Charybdis – that is to say, this model formally does not contradict to all the data. This, however, does not resolve the tension between the MINERνA and NOMAD neutrino data.

The remaining figures show the flux-folded CCQE and CCQE-like double-differential cross sections from the experiments MiniBooNE [30, 63] (Figs. 6 and 7), T2K ND 280 [73, 135] (Figs. 8, 9, and 10), and MINERνA [132, 139] (Figs. 11 and 12) along with predictions of the SM RFG + $M_A^{\rm run}$ and several other contemporary models. In calculations with the models incorporated into GENIE (SM RFG + $M_A^{\rm run}$ and physics tunes G18_10a_02_11a and G18_10b_02_11a[7]) we thoroughly accounted for all experimental cuts and real elemental compositions of the detectors. The results of all other models examined below are either obtained with the default GENIE 2 setting, or reproduced exactly as provided by the authors; the related references are given in the captions to the figures.

In the four self-explanatory accompanying tables 1 – 4 we summarize the χ^2/ndf values which provide quantitative comparison of the models under consideration with the data. Tables 1 and 2 also show the results of the analysis which accounts for the overall normalization uncertainties of the (anti)neutrino fluxes. The values denoted as χ^2_N/ndf (see definition (7) below) in the last columns are obtained after the best-fit renormalization of the model predictions to the data; the corresponding normalization factors, N, are listed in the third columns. As evident from the tables, the renormalization leads, as a rule, to an improvement of the χ^2/ndf values.

The comparisons with the MiniBooNE measurements [30, 63] shown in

[7] These tunes are based on the same physics, except for the applied FSI model: hA 2018 and hN 2018 for, respectively, G18_10a_02_11a and G18_10b_02_11a. Since the differences in the calculated cross sections due to the FSI effects forecast by the two models are comparatively small, we illustrate in the figures only one FSI model; the quantitative statistical characteristics for both models are listed in tables 1 – 4.

Figs. 6 and 7 and in table 1 suggest that the SM RFG + $M_A^{\rm run}$ model is in very good agreement with the data and has the least χ^2s for both ν_μ and $\overline{\nu}_\mu$ datasets. It should be reminded that the MiniBooNE collaboration does not provide information on the correlations of experimental uncertainties, so one must draw conclusions with care, even for the models having discrepancies with the data. Also recall that the MiniBooNE data were included into the global fit of the parameters M_0 and E_0, but this does not depreciate good agreement with the data, considering that the model practically does not require renormalization. This means the MiniBooNE data are matched by adjusting only a couple of parameters. Both GENIE 3 tunes and SuSAv2-MEC model show good agreement with the MiniBooNE data and require only modest renormalization within the reported experimental normalization uncertainty. The counterintuitively large χ^2 value for the GiBUU prediction for the ν_μ cross section, in comparison with, e.g., SuSAM* model which describes the ν_μ dataset far worse (by eye), is because of the systematic bias of the GiBUU curves from the data points at highest muon energies and at backward scattering angles, visually indistinguishable in the figure. However, for the $\overline{\nu}_\mu$ dataset, the GiBUU's χ^2 is almost the same as or even better than (after renormalization) that for the SM RFG + $M_A^{\rm run}$ model. The SuSAM* model experiences difficulties in accurately describing the MiniBooNE data.

Figure 8 and table 2 present a comparison of the model predictions with the flux-folded double-differential cross sections for the CCQE-like ("CC0π") ν_μ scattering from water target as measured by T2K ND280 [135]. In this case, we define

$$\chi^2_N = (\mathbf{E} - N\mathbf{T})^T \widetilde{\mathbf{W}}^{-1} (\mathbf{E} - N\mathbf{T}) + (N-1)^2/\delta^2 \quad \text{and} \quad \chi^2 \equiv \chi^2_1, \qquad (7)$$

where $\mathbf{E}$ and $\mathbf{T}$ are the vectors of the bin-averaged experimental data (E_i) and associated model predictions (T_i), respectively, $\widetilde{\mathbf{W}}$ is the full covariance matrix minus one that contains the bin-by-bin covariances related to the neutrino flux uncertainties, and $\delta \simeq 0.088$ is the overall flux normalization uncertainty. It is seen that the models under consideration are consistent with the data. The best agreement occurs for the two GENIE 3 tunes and the FSI effects simulated with the hA 2018 and hN 2018 models are practically indistinguishable. The χ^2 values for the SM RFG + $M_A^{\rm run}$ models (also very weakly dependent of the FSI effect modeling versions) are worse but entirely satisfactory and can be further improved by an 11% renormalization.

The state of affairs is much less satisfactory for the CCQE-like ν_μ scattering from a carbonaceous target studied in the recent T2K ND280 experi-

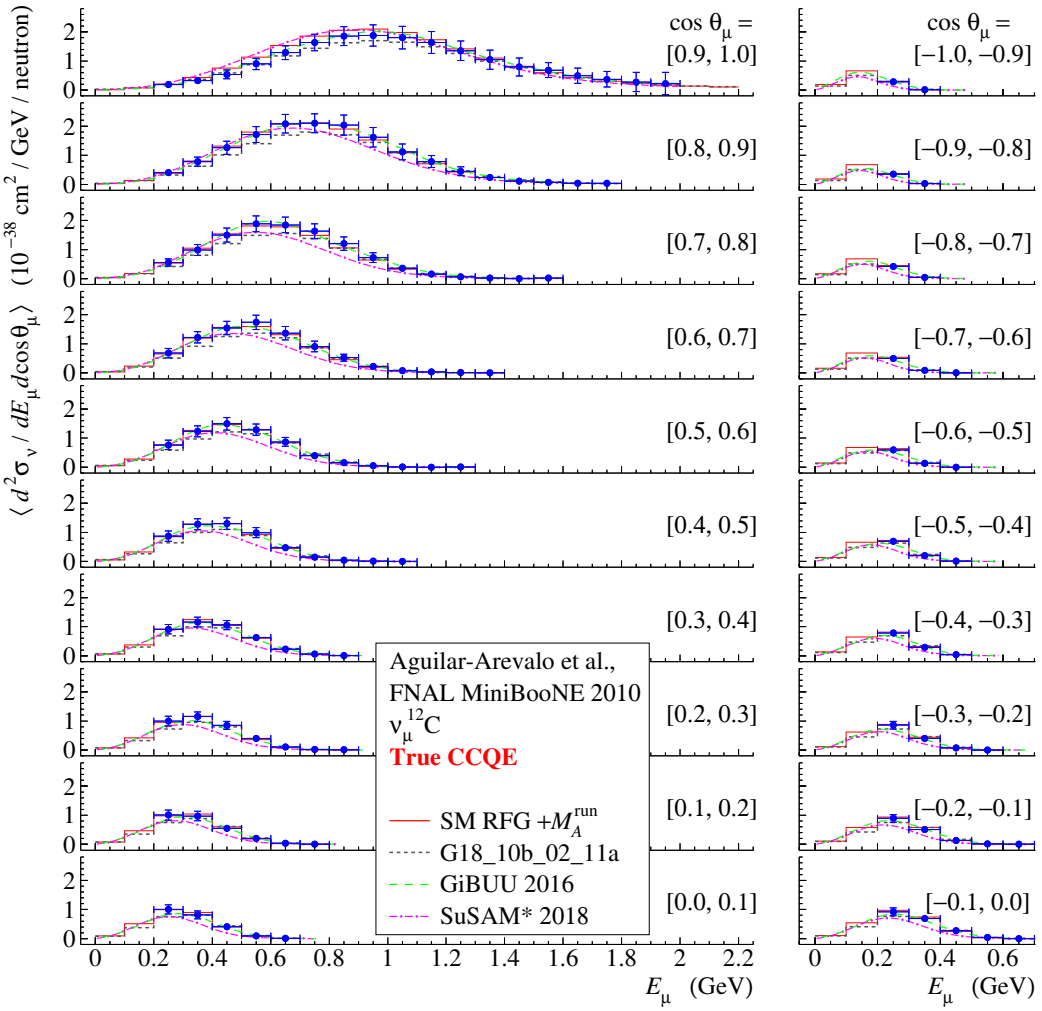

Figure 6: Flux-weighted double-differential cross section for the true CCQE ν_μ scattering from mineral oil as measured by MiniBooNE [30] and plotted vs. muon kinetic energy, E_μ, for several intervals of the cosine of muon scattering angle, θ_μ (shown in square brackets). Vertical error bars represent the total errors including the normalization uncertainty of 10.7% (due mainly to the NuMI ν_μ flux indetermination). The curves show predictions of the SM RFG + $M_A^{\rm run}$, GiBUU 2016 [154], and SuSAM* 2018 [102] models; the histograms represent the GENIE 3 physics tune G18_10b_02_11a. See table 1 for more details.

ment [73] (see Figs. 9 and 10, and table 2). Considering that this experiment, as well as the MINERνA experiments [132, 139] discussed below, does not

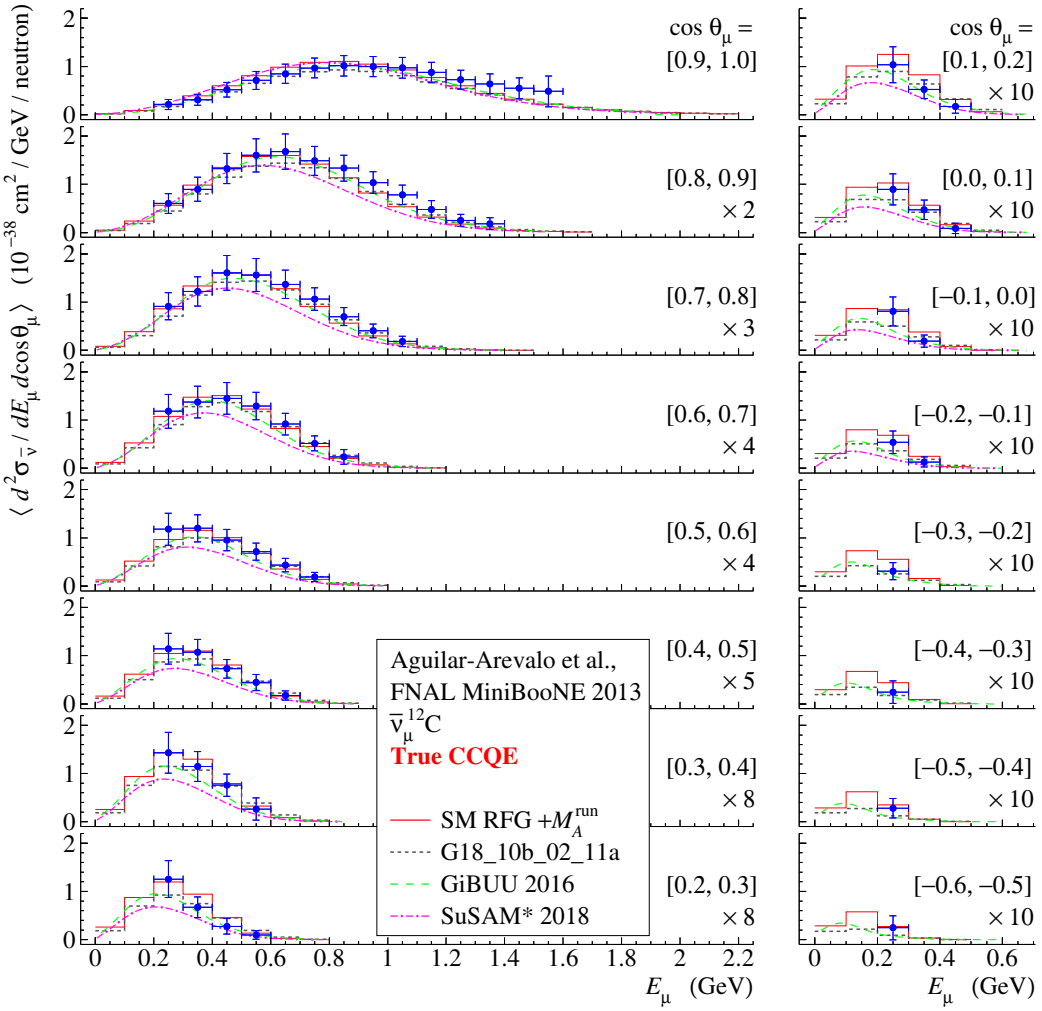

Figure 7: The same as in Fig. 6, but for $\overline{\nu}_\mu$ scattering [63]. Vertical error bars represent the total errors including the normalization uncertainty of 17.2% (due mainly to the NuMI $\overline{\nu}_\mu$ flux indetermination and conversion from the MiniBooNE mineral oil to carbon target). Some data are scaled for better visualization and the scale factors are indicated in the respective panels. See table 1 for more details.

provide the covariance matrix responsible for the flux uncertainties, one cannot unambiguously define the matrix $\widetilde{\mathbf{W}}$ (see eq. (7)) and thus it is difficult to properly define the normalization factor without loss of information on the bin-by-bin correlations. So to quantify the comparison, here and in the subsequent discussion we use the standard and log-normal least-squares cri-

Table 1: The absolute and relative (divided to the number of experimental bins, ndf) values of χ^2 calculated for the MiniBooNE neutrino and antineutrino CCQE datasets (see figs. 6 and 7) which include all sources of uncertainty but the relative normalization uncertainty δ; values of the normalization factors, N, obtained from the best fits to the data; and recalculated relative χ^2_N values found with taking into account the factors N in the penalty terms $(N-1)^2/\delta^2$. Calculations are done for the SM RFG + $M_A^{\rm run}$ model, GENIE 3 physics tune G18_10b_02_11a, two superscaling models SuSAv2-MEC 2016 [98] and SuSAM* 2018 [102], and also for GiBUU 2016 [154].

Model	$\frac{\chi^2}{\rm ndf}$	N	$\frac{\chi^2_N}{\rm ndf-1}$
FNAL MiniBooNE 2010, ν_μ, $\delta = 10.7\%$			
SM RFG + $M_A^{\rm run}$	$37.0/137 = 0.27$	0.98	0.25
G18_10b_02_11a tune	$133.0/137 = 0.97$	1.08	0.77
SuSAv2-MEC 2016	$231.5/137 = 1.69$	1.09	0.46
SuSAM* 2018	$646.6/137 = 4.72$	1.21	3.71
GiBUU 2016	$523.3/137 = 3.82$	0.92	3.53
FNAL MiniBooNE 2013, $\overline{\nu}_\mu$, $\delta = 17.2\%$			
SM RFG + $M_A^{\rm run}$	$44.5/\ 78 = 0.57$	0.99	0.57
G18_10b_02_11a tune	$48.4/\ 78 = 0.62$	1.11	0.37
SuSAv2-MEC 2016	$78.1/\ 78 = 1.00$	1.09	0.83
SuSAM* 2018	$195.8/\ 78 = 2.51$	1.24	1.60
GiBUU 2016	$57.0/\ 78 = 0.73$	1.13	0.41

teria:

$$\chi^2_{\rm st} = (\mathbf{E}-\mathbf{T})^T\,\mathbf{W}^{-1}\,(\mathbf{E}-\mathbf{T})\,, \quad \chi^2_{\rm log} = (\ln\mathbf{E}-\ln\mathbf{T})^T\,\mathbf{V}^{-1}\,(\ln\mathbf{E}-\ln\mathbf{T})\,,$$

where $\ln\mathbf{E}$ and $\ln\mathbf{T}$ are, respectively, the vectors with the components $\ln(E_i)$ and $\ln(T_i)$; $\mathbf{W} = ||W_{ij}||$ is the full covariance matrix and $\mathbf{V} = ||W_{ij}/E_iE_j||$.

It is seen from table 2 that no one model, including the default model from the T2K-tuned neutrino event generator NEUT 5.4.0 [157, 158], can accurately describe the T2K C_8H_8 data. The worst case occurs for the full T2K dataset where the correlations drastically increase χ^2s for all models. A detailed comparisons of several other models with the data has been already done in [73]. These models also result in rather large standard least-squares

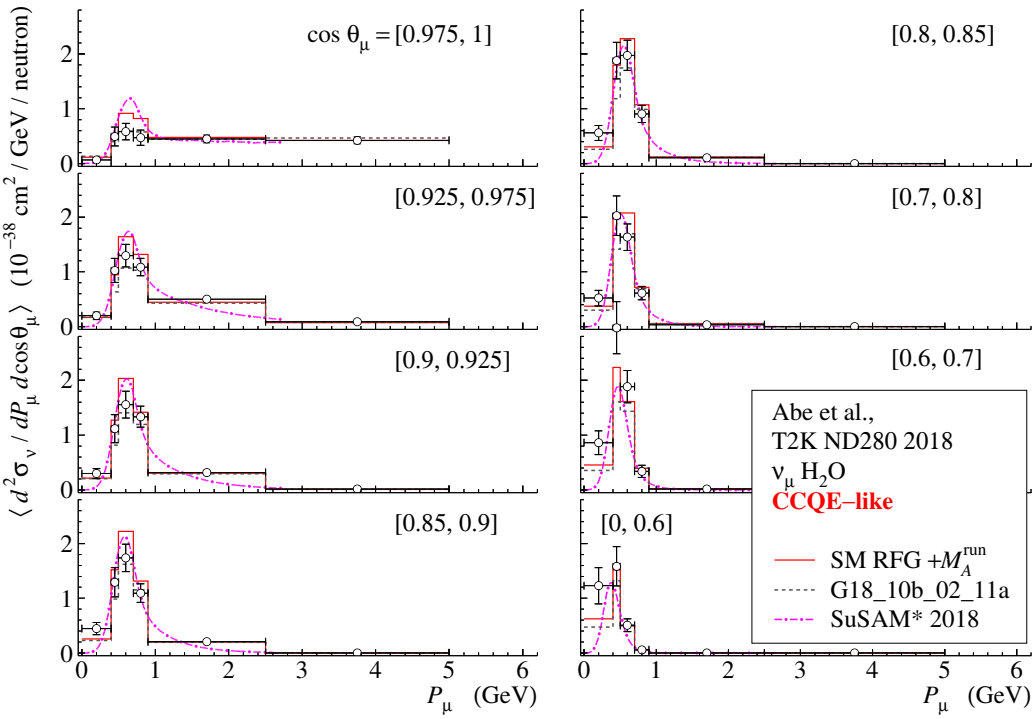

Figure 8: Flux-weighted double-differential cross sections for the CCQE-like ν_μ scattering from water target as measured by T2K ND280 [135] and plotted vs. muon momentum, P_μ, for several intervals of the cosine of muon scattering angle, θ_μ (shown in square brackets). Vertical error bars represent the total errors including the normalization uncertainty of 8.76%. Histograms represent the SM RFG + $M_A^{\rm run}$ model with the hN 2018 version of the FSI modeling and GENIE 3 physics tune G18_10b_02_11a; dashed-dotted curves show the SuSAM* 2018 [102] model prediction obtained with no account for the FSI effects. See table 2 for more details.

values for the full dataset: $\chi^2_{\rm st}/{\rm ndf} = 4 - 6.2$. As is argued in [73], this result should be treated with care. In particular, such $\chi^2_{\rm st}$ statistics can suffer from so-called Peelle's Pertinent Puzzle [159]. Recall that the SM RFG + $M_A^{\rm run}$ models and G18_10a/b_02_11a tunes satisfactory describe the T2K data on water target. If one ignores the theoretically expected small difference between the neutrino scattering on oxygen and carbon (isoscalar nuclei with close Z), the main distinctions between the two T2K measurements are in different event selection and data processing. Namely, in the T2K experiment with H_2O target [135] only the pionless ("CC-0π") events without protons in

Table 2: The same quantities as in table 1 but for the T2K ND280 CCQE-like dataset (measurements on a water target) [73]. The data are shown in Fig. 8. All calculations are done with the reduced covariance matrix $\widetilde{\mathbf{W}}$ for the SM RFG + $M_A^{\rm run}$ model with two versions of the FSI effects, GENIE 3 physics tunes G18_10a_02_11a and G18_10b_02_11a (in these cases the FSI effects lead to almost identical results), and SuSAM* 2018 model which neglects the FSI effects [102].

Model	$\frac{\chi^2}{\rm ndf}$	N	$\frac{\chi^2_N}{\rm ndf-1}$
SM RFG + $M_A^{\rm run}$ (hA 2018)	57.6/ 45 = 1.28	0.89	1.14
SM RFG + $M_A^{\rm run}$ (hN 2018)	57.6/ 45 = 1.30	0.89	1.16
G18_10a/b_02_11a tunes	49.5/ 45 = 1.01	1.03	1.02
SuSAM* 2018 (CCQE)	75.6/ 40 = 1.89	0.94	1.89

Table 3: Standard and log-normal χ^2/ndf calculated for the T2K ND280 neutrino CCQE-like datasets on the flux-weighted differential cross sections on hydrocarbon target [73] (see Figs. 9 and 10). Calculations are done for several models using the covariance matrices for the full T2K dataset (ndf = 93) and for a subset of the data dependent only on the leptonic variables (ndf = 60). Following to [73], only a part of the T2K data presented in Figs. 9 and 10 is included into the analysis. The number in parentheses for the T2K-tuned NEUT 5.4.0 model (incorporating a "LFG+RPA" model with $1p1h$ and $2p2h$ prediction by Nieves *et al.* [156]) is taken from ref. [73].

	Full dataset		Leptonic variables	
Model	$\frac{\chi^2_{\rm st}}{\rm ndf}$	$\frac{\chi^2_{\rm log}}{\rm ndf}$	$\frac{\chi^2_{\rm st}}{\rm ndf}$	$\frac{\chi^2_{\rm log}}{\rm ndf}$
SM RFG + $M_A^{\rm run}$ (hA 2018)	6.27	4.61	3.19	2.25
SM RFG + $M_A^{\rm run}$ (hN 2018)	5.77	4.45	3.39	2.93
GENIE 3 tune G18_10a_02_11a	4.19	4.46	2.17	2.87
GENIE 3 tune G18_10b_02_11a	4.22	4.51	2.18	2.90
T2K-tuned NEUT 5.4.0	(3.99)	4.63	2.90	3.77
GiBUU 2017 ($\mathcal{T}=0$)	—	—	2.83	2.45
GiBUU 2017 ($\mathcal{T}=1$)	—	—	3.90	2.75

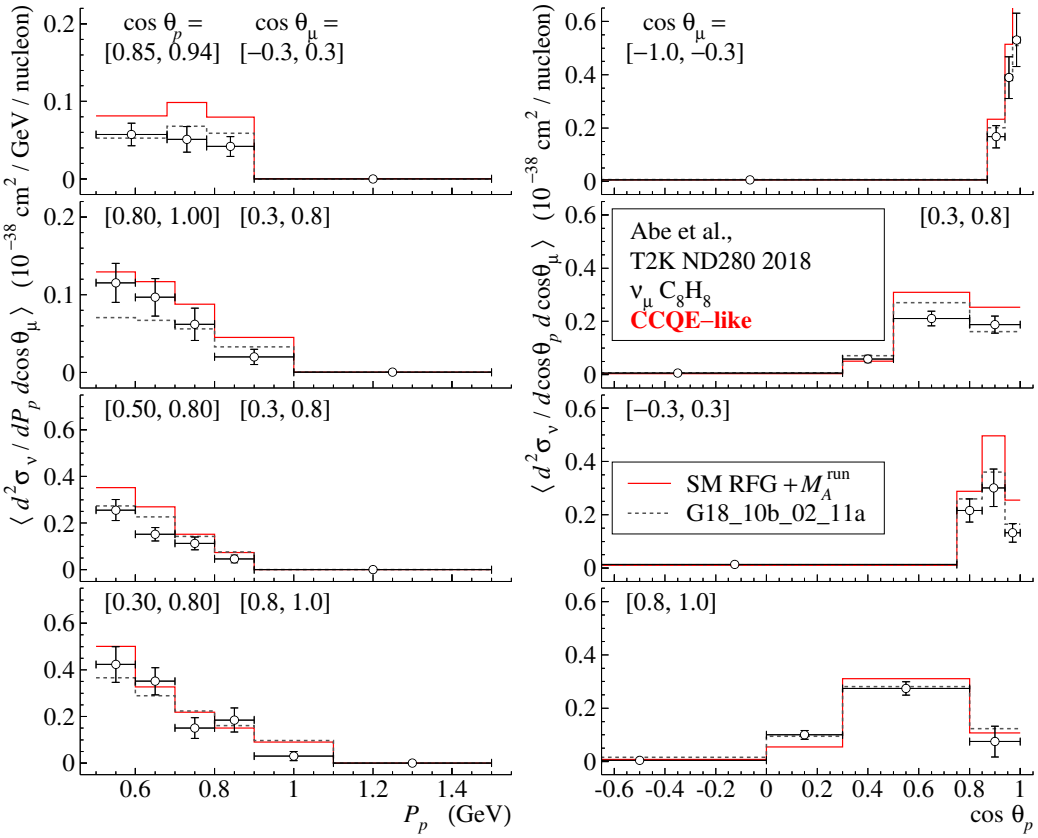

Figure 9: Flux-weighted double-differential cross sections for the CCQE-like ν_μ scattering from a carbonaceous target as measured by T2K ND280 [73] and plotted vs. proton momentum, P_p, for several intervals of cosines of proton and muon scattering angles, θ_p and θ_μ (four left panels); vs. $\cos\theta_p$ for several intervals of $\cos\theta_\mu$ (four right panels). All intervals of fixed angular variables are shown in square brackets. Vertical error bars represent the total errors including the normalization uncertainty of 8.5%. The histograms are calculated with SM RFG + M_A^{run} and GENIE 3 physics tune G18_10b_02_11a. See table 3 for details.

the final state were selected, while in the experiment with C_8H_8 target, the CC-0π events with the final-state protons having momenta above 500 MeV/c were included and classified by the number of protons (0, 1, and ≥ 2). What is more, the predicted cross sections in terms of muon variables (see Fig. 10) agree with the data better than ones for the data subset which include the final-state proton variables (Fig. 9). Hence we may suspect that the tremen-

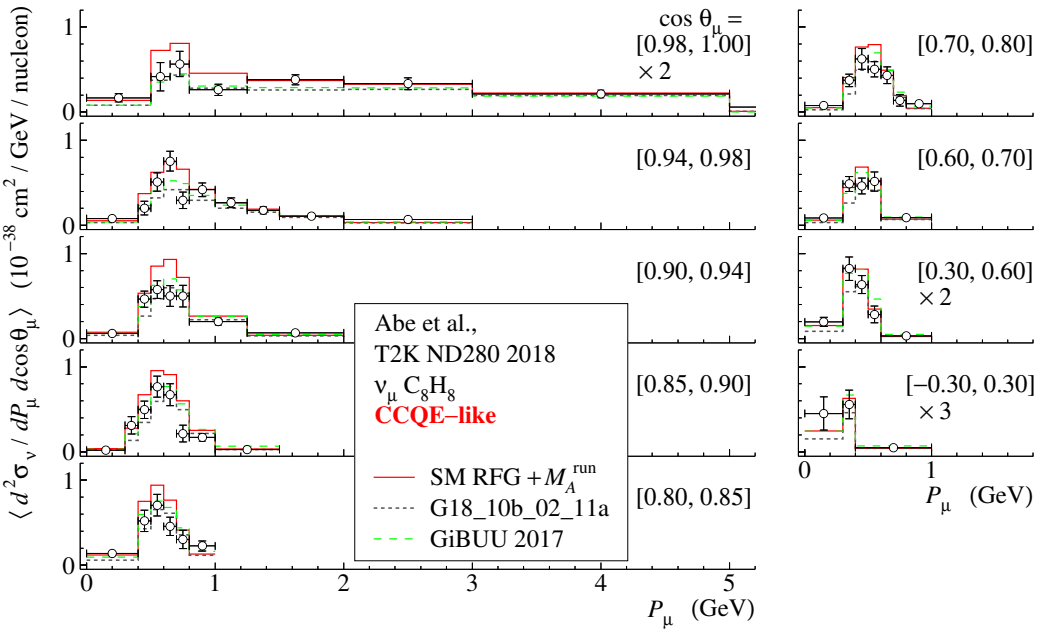

Figure 10: Flux-weighted double-differential cross sections for the CCQE-like ν_μ scattering from a carbonaceous target as measured by T2K ND280 [73] and plotted vs. muon momentum, P_μ, for several intervals of $\cos\theta_\mu$. All intervals of fixed angular variables are shown in square brackets. Vertical error bars represent the total errors including the normalization uncertainty of 8.5%. The histograms are calculated with SM RFG + $M_A^{\rm run}$, GiBUU 2017 ($\mathcal{T} = 0$) [155], and GENIE 3 physics tune G18_10b_02_11a. The data on two right bottom panels are scaled for better visualization and the scale factors are indicated in these panels. See table 3 for details.

dous disagreement between all the models and the T2K C_8H_8 data can be at least partially caused by the FSI problem.

Figures 11 and 12 show comparison of the flux-folded double-differential cross sections, $d^2\sigma/dP_T dP_L$, for the ν_μ and $\overline{\nu}_\mu$ CCQE scattering from hydrocarbon measured (applying several kinematic cuts) by MINERνA [132, 139] with some model predictions. Table 4 collects the standard and log-normal χ^2/ndf calculated for the more wide set of models for both CCQE and CCQE-like cross sections.

All the models under consideration, including the MINERνA-tuned GENIE 2.8.4 model are characterized by compatible $\chi^2_{\rm st}$ and $\chi^2_{\rm log}$ values, or, in other words, there is no unambiguously "best" model. There is a trend (al-

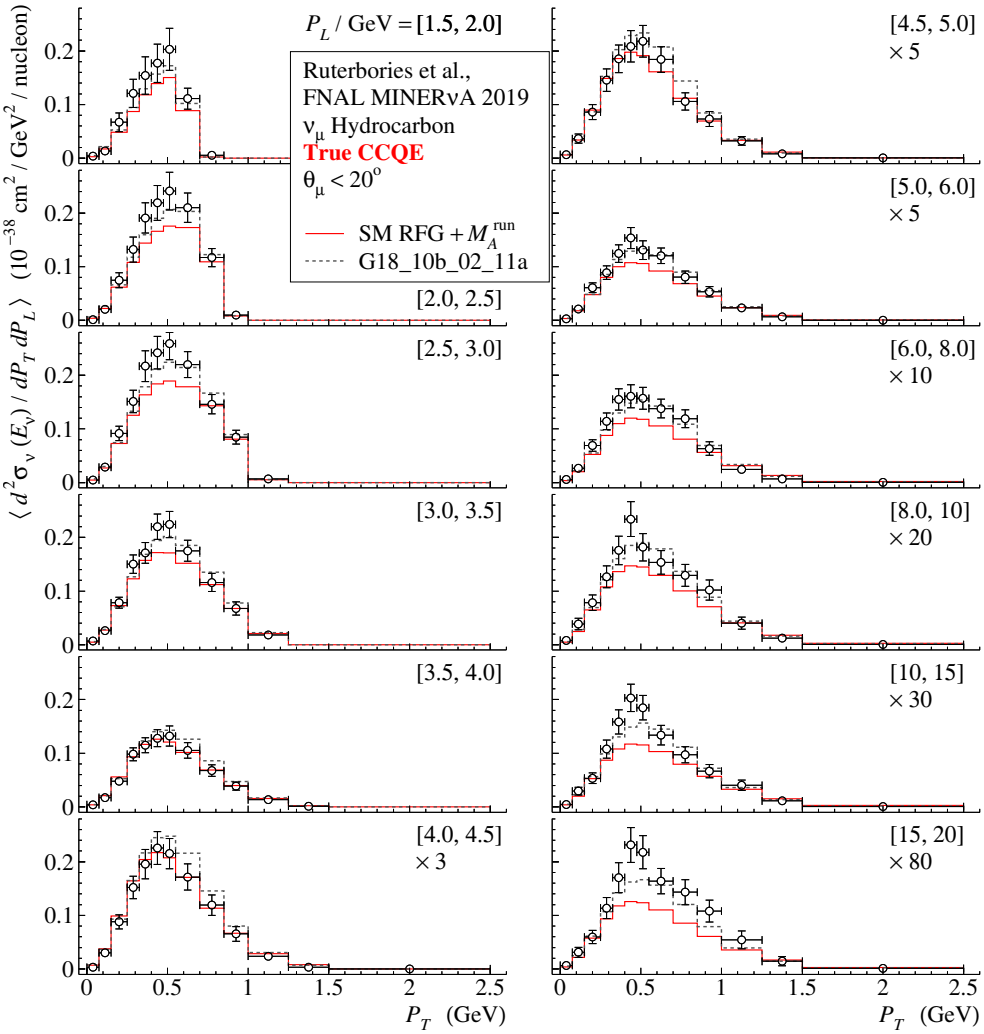

Figure 11: Flux-weighted double-differential cross sections for the CCQE ν_μ scattering from hydrocarbon as measured by MINERνA [139] and plotted vs. transverse muon momentum, P_T, for several intervals of longitudinal momentum, P_L (shown in square brackets). Vertical error bars represent the total errors including the normalization uncertainty. Applied kinematic cuts are explained in the main text. Histograms represent predictions of the SM RFG + $M_A^{\rm run}$ model and GENIE 3 physics tune G18_10b_02_11a. Some data are scaled for better visualization and the scale factors are indicated in the respective panels.

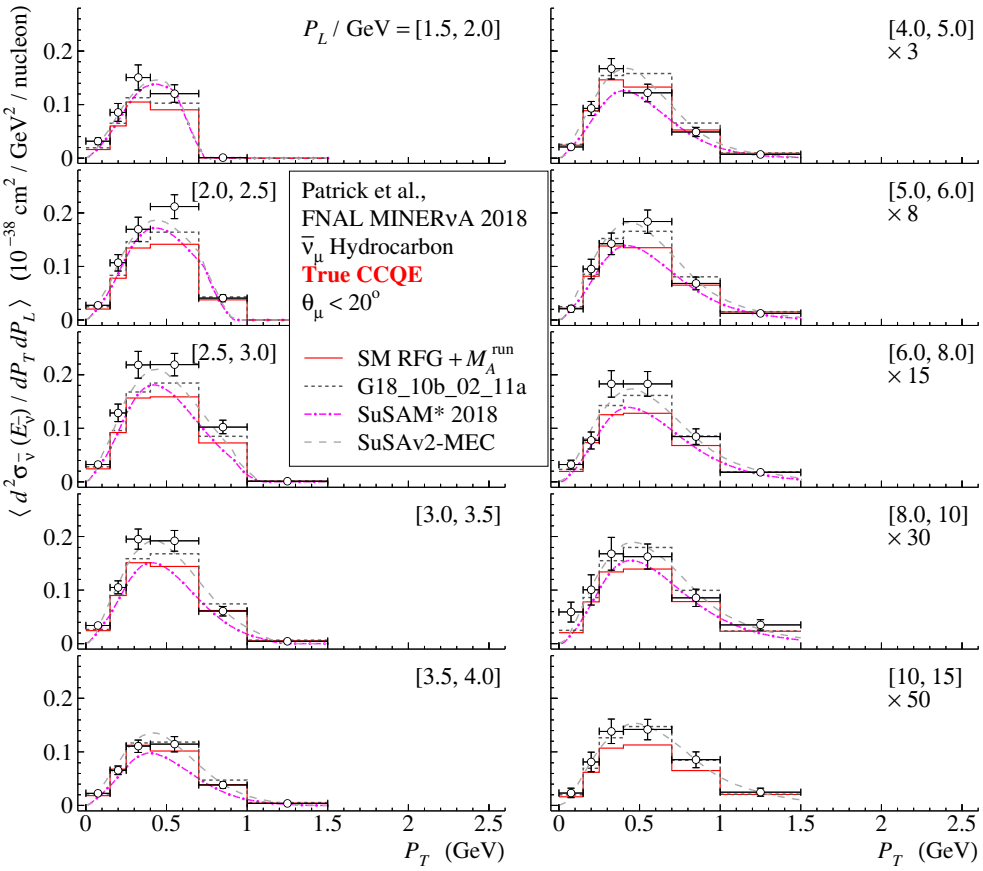

Figure 12: Flux-weighted double-differential cross sections for the CCQE $\overline{\nu}_\mu$ scattering from hydrocarbon as measured by MINERνA [132] and plotted vs. transverse muon momentum, P_T, for several intervals of longitudinal momentum, P_L (shown in square brackets). The notation for the data points and histograms is similar to that in Fig. 11. The dashed and dashed-dotted curves show predictions of the two superscaling models: SuSAv2-MEC [98] and SuSAM* [102], respectively. See table 4 for details to this and previous figure.

though not very distinct) toward increasing discrepancy with increase of the muon longitudinal momentum, P_L. The SM RFG + $M_A^{\rm run}$ model systematically underestimates the cross sections within their maxima but better agrees with the data in other kinematic regions. The GENIE 3 tunes and superscaling models better match the regions of maxima. This agrees with the data on the total CCQE cross sections shown in Fig. 5. Comparable values of the

Table 4: The values of the standard and log-normal χ^2/ndf calculated for the MINERνA neutrino [139] and antineutrino [132] CCQE and CCQE-like datasets on the flux-weighted double-differential cross sections $d^2\sigma/dP_T dP_L$. The CCQE data are shown in figs. 11 and 12. Calculations are done for several models using the full covariance matrices with degrees of freedom equal to 144 and 58 for ν_μ and $\overline{\nu}_\mu$ datasets, respectively. The MINERνA-tuned GENIE model [132, 139] incorporating RPA and tuned $2p2h$ has been used in the extracting the cross sections. Note that our estimation of the $\chi^2_{\rm st}$/ndf for the SuSAv2-MEC model [99] ($\overline{\nu}_\mu$ case) differs from author's result of 1.79.

Model	CCQE		CCQE-like	
	$\frac{\chi^2_{\rm st}}{\rm ndf}$	$\frac{\chi^2_{\rm log}}{\rm ndf}$	$\frac{\chi^2_{\rm st}}{\rm ndf}$	$\frac{\chi^2_{\rm log}}{\rm ndf}$
Neutrino dataset (ndf=144)				
SM RFG + $M_A^{\rm run}$ (hA 2018)	1.66	1.53	1.73	1.81
SM RFG + $M_A^{\rm run}$ (hN 2018)	1.65	1.52	1.49	1.86
GENIE 3 tune G18_10a_02_11a	1.43	1.20	1.48	1.32
GENIE 3 tune G18_10b_02_11a	1.45	1.22	1.26	1.34
MINERνA-tuned GENIE 2.8.4	1.51	1.04	1.77	1.41
Antineutrino dataset (ndf=58)				
SM RFG + $M_A^{\rm run}$ (hA 2018)	1.34	2.22	1.49	2.06
SM RFG + $M_A^{\rm run}$ (hN 2018)	1.34	2.11	1.49	2.14
GENIE 3 tune G18_10a_02_11a	1.46	1.89	1.44	1.74
GENIE 3 tune G18_10b_02_11a	1.44	1.85	1.40	1.72
SuSAv2-MEC 2018	2.13	2.02	—	—
SuSAM* 2018	1.51	2.64	—	—
MINERνA-tuned GENIE 2.8.4	1.58	1.85	1.40	1.70

standard and log-normal χ^2s indicate absence of anomalous data points. For the neutrino CCQE-like dataset there is noticeable difference in the FSI effects predicted by the hA 2018 and hN 2018 models and there is no significant difference for the antineutrino dataset.

5 Conclusions

We propose the notion of running (energy-dependent) axial-vector mass, $M_A^{\rm run}(E_\nu)$, to describe the CCQE interactions of neutrinos and antineutrinos with nuclei within the framework of the conventional RFG model by Smith and Moniz. This intention is inspired by purely heuristic fact that the effective (dipole) axial-vector mass of the nucleon reported in several recent experiments on CCQE and CCQE-like (anti)neutrino interactions with nuclei increases with decreasing the mean energy of the (anti)neutrino beams (see Fig. 2); it is *a posteriori* confirmed with an extended dataset (Fig. 4). We investigated the simplest ansatz for the function $M_A^{\rm run}(E_\nu)$ with only two adjustable parameters M_0 and E_0 independent of Z and A for $Z \geq 6$. The best-fit values of these parameters were derived from a global statistical analysis of all available self-consistent CCQE data for substantial variety of nuclear targets and $\nu/\overline{\nu}$ energy spectra (see sect. 3). The best-fit value of M_0 is in very good agreement with the axial mass value extracted from deuterium data as well as with the results of the earlier global analyses [54, 58] and thus it can be treated as the improved world average of the conventional axial-vector mass of the nucleon.

The model is in very good agreement with the earlier data, including the data from NOMAD and MiniBooNE. Also it has been tested against the most recent results of the experiments MINERνA and T2K and, with certain reservations, shows reasonable agreement with the data. More specifically, it somewhat underestimates the MINERνA data providing a hint to a tension between the MINERνA results with the previous measurements in the overlapping energy ranges (SKAT, LAr-TPC, NOMAD, and others). Certainly no model is capable to precisely describe both the MINERνA and earlier neutrino datasets (a meaningful example is shown in Fig. 5). Due to very different $\nu/\overline{\nu}$ energy spectra in the MiniBooNE and T2K experiments, the direct comparison of their outputs is difficult; our model provides a tool for such a comparison which in particular shows that the results of MiniBooNE [30] (mineral oil) and T2K ND280 [135] (water target) are largely consistent with each other. Much worse situation is observed with the T2K 2018 data on carbonaceous target [73]. The worst inconsistency occurs with the T2K 2018 distributions over the final-state proton variables which, however, provide certain difficulty as well for all other tested models (including the model tuned to the T2K data), even after applying the renormalization procedure (see sect. 4). It is thought that the discrepancies are at least in

part due to the incompleteness of the FSI models implemented into the neutrino generators, but can also be attributed to the T2K data themselves. In other words the suggested model has a statistical quality comparable to that of more involved microscopic models.

The best-fit values of M_0 and E_0 are of course sensitive to the dataset involved into the statistical analysis and somewhat responsive to variations of the input parameters of the RFG model (Fermi momenta, separation energies) and the models for the nucleon electromagnetic form factors. However the analysis can almost automatically be repeated with extended datasets, and implementing any modifications of the RFG model (e.g., Bodek–Ritchie RFG) or its extensions (SF, LFG, etc.), as well as with the more advanced nuclear models. A more complex parametrization of the function $M_A^{\mathrm{run}}(E_\nu)$ seems to be unreasonable for the present-day level of accuracy and consistency of the CCQE and CCQE-like data but may be needed in the future. Individual parametrizations for different nuclei or nuclear groups are also unreasonable today; this is because the currently available dataset for the inorganic heavy nuclear targets is not sufficiently accurate and self-consistent. There is no statistically significant difference between the M_A^{run} parameters extracted separately from the ν_μ and $\overline{\nu}_\mu$ data, but there is a hint to possible difference. Any case, the available $\overline{\nu}_\mu$ dataset is not yet sufficient for a more definite statement. To draw more robust conclusions it is desirable to compare our predictions with the T2K antineutrino data and MINERνA data for a broader-spectrum beam peaking around 6 GeV and to add the new data into the global fit. All details of the analysis and more comprehensive comparison with the experimental data will be discussed in a posterior paper.

We thank to Ulrich Mosel, Stephen Dolan, Jose Amaro, and Ignacio Ruiz Simo for providing us with the scripts and tabulated data for their models. We are very grateful to Samoil Bilenky, Arie Bodek, Dmitry Naumov, Kendall Mahn, Alexander Olshevskiy, Olga Petrova, Oleg Samoylov, Oleg Teryaev, and our colleagues from the GENIE Collaboration for helpful discussions and critical comments. Research of I. K. has been supported by the Russian Science Foundation grant No. 18-12-00271.

References

[1] E. Fernandez-Martinez and D. Meloni. Importance of nuclear effects in the measurement of neutrino oscillation parameters. *Phys. Lett.*, B

697:477–481, 2011.

[2] D. Meloni. Impact of nuclear effects in the measurement of neutrino oscillation parameters. *AIP Conf. Proc.*, 1405:65–70, 2011.

[3] S. Chauhan, M. Sajjad Athar, and S. K. Singh. Nuclear effects in neutrino oscillation experiments. *AIP Conf. Proc.*, 1382:38–41, 2011.

[4] D. Meloni and M. Martini. Revisiting the T2K data using different models for the neutrino-nucleus cross sections. *Phys. Lett.*, B 716:186–192, 2012.

[5] O. Benhar and N. Rocco. Nuclear effects in neutrino interactions and their impact on the determination of oscillation parameters. *Adv. High Energy Phys.*, 2013:912702, 2013.

[6] D. Meloni. Impact of nuclear effects in the measurement of neutrino oscillation parameters. *J. Phys. Conf. Ser.*, 408:012024, 2013.

[7] P. Coloma and P. Huber. Impact of nuclear effects on the extraction of neutrino oscillation parameters. *Phys. Rev. Lett.*, 111:221802, 2013.

[8] P. Coloma, P. Huber, C.-M. Jen, and C. Mariani. Neutrino-nucleus interaction models and their impact on oscillation analyses. *Phys. Rev.*, D 89:073015, 2014.

[9] C.-M. Jen, A. Ankowski, O. Benhar, A. P. Furmanski, L. N. Kalousis, and C. Mariani. Numerical implementation of lepton-nucleus interactions and its effect on neutrino oscillation analysis. *Phys. Rev.*, D 90:093004, 2014.

[10] P. Stowell, C. Wilkinson, and S. Cartwright. Effect of cross-section models on the validity of sterile neutrino mixing limits, 2015. arXiv:1501.02142 [hep-ph].

[11] M. Ericson and M. Martini. Neutrino versus antineutrino cross sections and CP violation. *Phys. Rev.*, C 91:035501, 2015.

[12] A. M. Ankowski, O. Benhar, C. Mariani, and E. Vagnoni. Effect of the $2p2h$ cross-section uncertainties on an analysis of neutrino oscillations. *Phys. Rev.*, D 93:113004, 2016.

[13] L. D. Kolupaeva, K. S. Kuzmin, O. N. Petrova, and I. M. Shandrov. Some uncertainties of neutrino oscillation effect in the NOνA experiment. *Mod. Phys. Lett.*, A 31(12):1650077, 2016.

[14] A. M. Ankowski and C. Mariani. Systematic uncertainties in long-baseline neutrino-oscillation experiments. *J. Phys.*, G 44(5):054001, 2017.

[15] K. S. Kuzmin, V. A. Naumov, and O. N. Petrova. Running axial mass of the nucleon for the NOνA experiment. *Acta Phys. Polon. Supp.*, 9:795–796, 2016.

[16] R. L. Kustom, D. E. Lundquist, T. B. Novey, A. Yokosawa, and F. Chilton. Quasielastic neutrino scattering. *Phys. Rev. Lett.*, 22:1014–1017, 1969.

[17] W. A. Mann et al. Study of the reaction $\nu + n \to \mu^- + p$. *Phys. Rev. Lett.*, 31:844–847, 1973.

[18] D. H. Perkins. Review of neutrino experiments. In T. W. Kirk, editor, *Proceedings of the International Symposium on Lepton and Photon Interactions at High Energies, Leland Stanford Junior University, Stanford, California, USA, August 21–27, 1975*, pages 571–603, Stanford, 1976. SLAC.

[19] S. J. Barish et al. Study of neutrino interactions in hydrogen and deuterium: Description of the experiment and study of the reaction $\nu + d \to \mu^- + p + p_s$. *Phys. Rev.*, D 16(11):3103–3121, 1977.

[20] K. L. Miller et al. Study of the reaction muon-neutrino $\nu_\mu d \to \mu^- p p_s$. *Phys. Rev.*, D 26(3):537–542, 1982.

[21] A. M. Cnops et al. Neutrino-deuterium reactions in the 7-ft bubble chamber. In A. G. Michette and P. B. Renton, editors, *Proceedings of the Topical Conference on Neutrino Physics at Accelerators, Oxford, England, UK, July 4–7, 1978*, pages 62–67, Chilton, England, UK, 1978. Science Research Council, Rutherford Laboratory.

[22] G. K. Fanourakis, L. K. Resvanis, G. A. Grammatikakis, P. Tsilimigras, A. Vayaki, U. Camerini, W. F. Fry, R. J. Loveless, J. H. Mapp,

and D. D. Reeder. Study of low-energy anti-neutrino interactions on protons. *Phys. Rev.*, D 21(3):562–568, 1980.

[23] N. J. Baker et al. Quasielastic neutrino scattering: A Measurement of the weak nucleon axial vector form-factor. *Phys. Rev.*, D 23(11):2499–2505, 1981.

[24] L. A. Ahrens et al. A study of the axial vector form-factor and second class currents in anti-neutrino quasielastic scattering. *Phys. Lett.*, B 202:284–288, 1988.

[25] T. Kitagaki et al. Study of neutrino $\nu d \to \mu^- p p_s$ and $\nu d \to \mu^- \Delta^{++}(1232) n_s$ using the BNL 7-foot deuterium filled bubble chamber. *Phys. Rev.*, D 42(5):1331–1338, 1990.

[26] T. Kitagaki et al. High-energy quasielastic $\nu_\mu n \to \mu^- p$ scattering in deuterium. *Phys. Rev.*, D 28(3):436–442, 1983.

[27] A. E. Asratian et al. Anti-neutrinos quasielastic scattering in neon and total cross-sections in the energy interval 10–50 GeV. *Sov. J. Nucl. Phys.*, 39:392–395, 1984.

[28] A. E. Asratian et al. Total anti-neutrinos nucleon charged current cross-section in the energy range 10–50 GeV. *Phys. Lett.*, B 137:122–124, 1984.

[29] V. V. Ammosov et al. Neutral strange particle exclusive production in charged current high-energy anti-neutrino interactions. *Z. Phys.*, C 36:377–381, 1987.

[30] A. A. Aguilar-Arevalo et al. First measurement of the muon neutrino charged current quasielastic double differential cross section. *Phys. Rev.*, D 81:092005, 2010.

[31] M. Betancourt. *Study of the quasi-elastic scattering in the NOνA detector prototype*. PhD thesis, Minnesota University, 2013.

[32] M. Holder et al. Spark-chamber study of elastic neutrino interactions. *Nuovo Cim.*, A 57(2):338–354, 1968.

[33] C. Franzinetti. *Neutrino interactions in the CERN heavy liquid bubble chamber*. Number CERN Yellow Report No. 66–13. CERN, Geneva, 1965. Lecture at the Meeting of the American Physical Society, Chicago, October 28, 1965.

[34] E. C. M. Young. High-energy neutrino interactions. Technical report, CERN, 1967. CERN Yellow Report No. 67–12.

[35] A. Orkin-Lecourtois and C. A. Piketty. The quasi-elastic events of the CERN bubble chamber neutrino experiment and the determination of the axial form factor. *Nuovo Cim.*, A 50(4):927–934, August 1967.

[36] I. Budagov et al. A study of the elastic neutrino process $\nu + n \to \mu^- + p$. *Lett. Nuovo Cim.*, 2:689–695, 1969.

[37] S. Bonetti, G. Carnesecchi, D. Cavalli, P. Negri, A. Pullia, M. Rollier, F. Romano, and R. Schira. Study of quasielastic reactions of neutrino and anti-neutrino in Gargamelle. *Nuovo Cim.*, A 38:260–270, 1977.

[38] M. Rollier. Recent results from the Gargamelle anti-neutrino propane experiment at the CERN PS. In A. G. Michette and P. B. Renton, editors, *Neutrino physics at accelerators, Topical Conference on Neutrino Physics, July 4–7, 1978. Oxford, England, UK*, pages 68–74, Chilton, England, UK, 1978. Science Research Council, Rutherford Laboratory.

[39] N. Armenise et al. Charged current elastic anti-neutrino interactions in propane. *Nucl. Phys.*, B 152:365–375, 1979.

[40] M. Pohl et al. Experimental study of the reaction $\nu n \to \mu^- p$. *Lett. Nuovo Cim.*, 26:332–336, 1979.

[41] D. Allasia et al. Investigation of exclusive channels in $\nu/\overline{\nu}$-deuteron charged current interactions. *Nucl. Phys.*, B 343:285–309, 1990.

[42] V. V. Lyubushkin et al. A study of quasi-elastic muon neutrino and antineutrino scattering in the NOMAD experiment. *Eur. Phys. J.*, C 63:355–381, 2009.

[43] V. V. Makeev et al. Quasielastic neutrino scattering $\nu_\mu + n \to \mu^- + p$ at 2–20 GeV in bubble chamber SKAT. *JETP Lett.*, 34:397–400, 1981.

[44] H. J. Grabosch et al. Study of quasielastic reactions $\nu n \to \mu^- p$ and $\overline{\nu} p \to \mu^+ n$ in bubble chamber SKAT at 3–20 GeV. *Sov. J. Nucl. Phys.*, 47:1630–1634, 1988.

[45] J. Brunner et al. Quasielastic nucleon and hyperon production by neutrinos and anti-neutrinos with energies below 30 GeV. *Z. Phys.*, C 45:551–555, 1990.

[46] V. V. Ammosov et al. Investigation of neutrino interactions using the bubble chamber SKAT. *Sov. J. Part. Nucl.*, 23:283–316, 1992.

[47] S. V. Belikov et al. Quasielastic neutrino and anti-neutrinos interaction at the Serpukhov accelerator. Technical Report IFVE-81-146, Institute for High Energy Physics, Serpukhov, 1981.

[48] S. V. Belikov et al. Quasielastic $\nu_\mu n$ scattering at 3–30 GeV energy. *Sov. J. Nucl. Phys.*, 35:35–39, 1982.

[49] S. V. Belikov, A. A. Volkov, V. I. Kochetkov, A. I. Mukhin, Yu. M. Sviridov, and K. E. Shestermanov. Restraints on parameters of oscillations of muon neutrinos from quasielastic scattering data. *Sov. J. Nucl. Phys.*, 41:589, 1985.

[50] S. V. Belikov et al. Quasielastic neutrino and anti-neutrinos scattering: total cross-sections, axial vector form-factor. *Z. Phys.*, A 320:625–633, 1985.

[51] K. Abe et al. Measurement of the ν_μ charged-current quasielastic cross section on carbon with the ND280 detector at T2K. *Phys. Rev.*, D 92:112003, 2015.

[52] V. Bernard, L. Elouadrhiri, and Ulf-G. Meißner. Axial structure of the nucleon: Topical review. *J. Phys.*, G 28:R1–R35, 2002.

[53] A. Bodek, S. E. Avvakumov, R. K. Bradford Jr., and H. S. Budd. Modeling atmospheric neutrino interactions: Duality constrained parameterization of vector and axial nucleon form factors, 2007.

[54] A. Bodek, S. E. Avvakumov, R. K. Bradford Jr., and H. S. Budd. Vector and axial nucleon form factors: A duality constrained parameterization. *Eur. Phys. J.*, C 53:349–354, 2008.

[55] A. Bodek, S. E. Avvakumov, R. K. Bradford Jr., and H. S. Budd. Extraction of the axial nucleon form-factor from neutrino experiments on deuterium. *J. Phys. Conf. Ser.*, 110:082004, 2008.

[56] K. S. Kuzmin, V. V. Lyubushkin, and V. A. Naumov. Fine-tuning parameters to describe the total charged-current neutrino-nucleon cross section. *Phys. Atom. Nucl.*, 69:1857–1871, 2006.

[57] K. S. Kuzmin, V. V. Lyubushkin, and V. A. Naumov. Axial masses in quasielastic neutrino scattering and single-pion neutrinoproduction on nucleons and nuclei. *Acta Phys. Polon.*, B 37:2337–2348, 2006.

[58] K. S. Kuzmin, V. V. Lyubushkin, and V. A. Naumov. Quasielastic axial-vector mass from experiments on neutrino-nucleus scattering. *Eur. Phys. J.*, C 54:517–538, 2008.

[59] S. K. Singh. The effect of final state interactions and deuteron binding in $\nu d \to \mu^- pp^*$. *Nucl. Phys.*, B 36:419–435, 1972.

[60] S. K. Singh. Quasielastic neutrino-deuteron scattering. *Phys. Rev.*, D 10(3):988–992, 1974.

[61] S. K. Singh and H. Arenhovel. Pion exchange current effects in $\nu_\mu + d \to \mu^- + p + p$. *Z. Phys.*, A 324:347–354, 1986.

[62] R. A. Smith and E. J. Moniz. Neutrino reactions on nuclear targets. *Nucl. Phys.*, B 43:605–622, 1972.

[63] A. A. Aguilar-Arevalo et al. First measurement of the muon antineutrino double-differential charged-current quasielastic cross section. *Phys. Rev.*, D 88:032001, 2013.

[64] J. L. Alcaraz-Aunion and J. Walding. Measurement of the ν_{mu}-CCQE cross section in the SciBooNE experiment. *AIP Conf. Proc.*, 1189:145–150, 2009.

[65] J. L. Alcaraz Aunion. *Measurement of the absolute ν_μ-CCQE cross section at the SciBooNE experiment.* PhD thesis, Barcelona, IFAE, 2010.

[66] G. A. Fiorentini et al. Measurement of muon neutrino quasielastic scattering on a hydrocarbon target at $E_\nu \sim 3.5$ GeV. *Phys. Rev. Lett.*, 111:022502, 2013.

[67] L. Fields et al. Measurement of muon antineutrino quasielastic scattering on a hydrocarbon target at $E_\nu \sim 3.5$ GeV. *Phys. Rev. Lett.*, 111:022501, 2013.

[68] T. Walton et al. Measurement of muon plus proton final states in ν_μ interactions on hydrocarbon at $\langle E_\nu \rangle = 4.2$ GeV. *Phys. Rev.*, D 91:071301, 2015.

[69] P. Adamson et al. Study of quasielastic scattering using charged-current ν_μ-iron interactions in the MINOS near detector. *Phys. Rev.*, D 91:012005, 2015.

[70] K. Abe et al. Measurement of the inclusive ν_μ charged current cross section on carbon in the near detector of the T2K experiment. *Phys. Rev.*, D 87:092003, 2013.

[71] D. Hadley. Measurement of the ν_μ CCQE cross section with the ND280 detector at T2K. *PoS(EPS-HEP 2013)008*.

[72] K. Abe et al. Measurement of double-differential muon neutrino charged-current interactions on C_8H_8 without pions in the final state using the T2K off-axis beam. *Phys. Rev.*, D 93:112012, 2016.

[73] K. Abe et al. Characterization of nuclear effects in muon-neutrino scattering on hydrocarbon with a measurement of final-state kinematics and correlations in charged-current pionless interactions at T2K. *Phys. Rev.*, D 98(3):032003, 2018.

[74] K. Abe et al. Measurement of the ν_μ charged current quasielastic cross section on carbon with the T2K on-axis neutrino beam. *Phys. Rev.*, D 91:112002, 2015.

[75] A. V. Butkevich and D. Perevalov. Determination of the axial nucleon form factor from the MiniBooNE data. *Phys. Rev.*, D 89:053014, 2014.

[76] R. W. Gran et al. Measurement of the quasi-elastic axial vector mass in neutrino-oxygen interactions. *Phys. Rev.*, D 74:052002, 2006.

[77] X. Espinal and F. N. Sánchez. Measurement of the axial vector mass in neutrino-carbon interactions at K2K. *AIP Conf. Proc.*, 967:117–122, 2007.

[78] A. M. Sajjad, F. Akbar, A. M. Rafi, S. Chauhan, S. K. Singh, and F. Zaidi. Lepton production cross sections in quasielastic $\nu/\overline{\nu}-$A scattering, 2016. arXiv:1611.07166 [nucl-th].

[79] K. M. Graczyk. Local density and the RPA corrections in charge current quasielastic neutrino on oxygen, argon and iron scattering, 2004. nucl-th/0401053.

[80] A. M. Ankowski. Consistent analysis of neutral- and charged-current neutrino scattering off carbon. *Phys. Rev.*, C 86:024616, 2012.

[81] M. V. Ivanov, A. N. Antonov, J. A. Caballero, G. D. Megias, M. B. Barbaro, E. Moya de Guerra, and J. M. Udías. Charged-current quasielastic neutrino cross sections on ^{12}C with realistic spectral and scaling functions. *Phys. Rev.*, C 89(1):014607, 2014.

[82] A. Bodek, M. E. Christy, and B. Coopersmith. Effective spectral function for quasielastic scattering on nuclei. *Eur. Phys. J.*, C 74(10):3091, 2014.

[83] J. E. Sobczyk. Intercomparison of lepton-nucleus scattering models in the quasielastic region. *Phys. Rev.*, C 96(4):045501, 2017.

[84] M. V. Ivanov, A. N. Antonov, G. D. Megias, J. A. Caballero, M. B. Barbaro, J. E. Amaro, I. Ruiz Simo, T. W. Donnelly, and J. M. Udías. Realistic spectral function model for charged-current quasielastic-like neutrino and antineutrino scattering cross sections on ^{12}C. *Phys. Rev.*, C 99(1):014610, 2019.

[85] M. V. Ivanov, A. N. Antonov, G. D. Megias, J. A. Caballero, M. B. Barbaro, J. E. Amaro, I. Ruiz Simo, T. W. Donnelly, and J. M. Udías. Charged-current quasielastic (anti)neutrino cross sections on ^{12}C with realistic spectral functions including meson-exchange contributions. *AIP Conf. Proc.*, 2075(1):070004, 2019.

[86] M. B. Barbaro, J. E. Amaro, J. A. Caballero, T. W. Donnelly, and J. M. Udias. Relativistic models for quasi-elastic neutrino-nucleus scattering. *AIP Conf. Proc.*, 1441:417–419, 2012.

[87] A. Meucci and C. Giusti. Relativistic Green's function model in charged-current quasielastic neutrino and antineutrino scattering at MINERνA kinematics. *Phys. Rev.*, D 89(11):117301, 2014.

[88] R. W. Gran, J. M. Nieves, F. N. Sánchez, and M. J. Vicente Vacas. Neutrino-nucleus quasi-elastic and $2p2h$ interactions up to 10 GeV. *Phys. Rev.*, D 88(11):113007, 2013.

[89] T. Van Cuyck, N. Jachowicz, R. González-Jiménez, M. Martini, V. Pandey, J. Ryckebusch, and N. Van Dessel. Influence of short-range correlations in neutrino-nucleus scattering. *Phys. Rev.*, C 94(2):024611, 2016.

[90] J. M. Nieves, I. Ruiz Simo, and M. J. Vicente Vacas. Two particle-hole excitations in charged current quasielastic antineutrino–nucleus scattering. *Phys. Lett.*, B 721:90–93, 2013.

[91] V. Pandey, N. Jachowicz, J. Ryckebusch, T. Van Cuyck, and W. Cosyn. Quasielastic contribution to antineutrino-nucleus scattering. *Phys. Rev.*, C 89(2):024601, 2014.

[92] O. D. Lalakulich, U. Mosel, and K. Gallmeister. Energy reconstruction in quasielastic scattering in the MiniBooNE and T2K experiments. *Phys. Rev.*, C 86:054606, 2012.

[93] U. Mosel and K. Gallmeister. Muon-neutrino-induced charged current cross section without pions: Theoretical analysis. *Phys. Rev.*, C 97(4):045501, 2018.

[94] A. Bodek, H. S. Budd, and M. E. Christy. Neutrino quasielastic scattering on nuclear targets: parametrizing transverse enhancement (meson exchange currents). *Eur. Phys. J.*, C 71:1726, 2011.

[95] J. T. Sobczyk. Transverse enhancement model and MiniBooNE charge current quasi-elastic neutrino scattering data. *Eur. Phys. J.*, C 72:1850, 2012.

[96] J. E. Amaro, M. B. Barbaro, J. A. Caballero, T. W. Donnelly, and C. F. Williamson. Meson-exchange currents and quasielastic neutrino cross sections in the SuperScaling approximation model. *Phys. Lett.*, B 696:151–155, 2011.

[97] R. Gonzaléz-Jiménez, G. D. Megias, M. B. Barbaro, J. A. Caballero, and T. W. Donnelly. Extensions of superscaling from relativistic mean field theory: the SuSAv2 model. *Phys. Rev.*, C 90(3):035501, 2014.

[98] G. D. Megias, J. E. Amaro, M. B. Barbaro, J. A. Caballero, T. W. Donnelly, and I. Ruiz Simo. Charged-current neutrino-nucleus reactions within the superscaling meson-exchange current approach. *Phys. Rev.*, D 94(9):093004, 2016.

[99] G. D. Megias, M. B. Barbaro, J. A. Caballero, and S. Dolan. Analysis of the MINERvA antineutrino double-differential cross sections within the SuSAv2 model including meson-exchange currents. *Phys. Rev.*, D 99(11):113002, 2019.

[100] J. E. Amaro, M. B. Barbaro, J. A. Caballero, R. González-Jiménez, G. D. Megias, and I. Ruiz Simo. Electron- versus neutrino-nucleus scattering. 2019. arXiv:1912.10612 [nucl-th].

[101] J. E. Amaro, E. Ruiz Arriola, and I. Ruiz Simo. Scaling violation and relativistic effective mass from quasi-elastic electron scattering: Implications for neutrino reactions. *Phys. Rev.*, C 92(5):054607, 2015.

[102] I. Ruiz Simo, V. L. Martinez-Consentino, J. E. Amaro, and E. Ruiz Arriola. Quasielastic charged-current neutrino scattering in the scaling model with relativistic effective mass. *Phys. Rev.*, D 97(11):116006, 2018.

[103] S. Boyd, S. Dytman, E. Hernandez, J. Sobczyk, and R. Tacik. Comparison of models of neutrino-nucleus interactions. *AIP Conf. Proc.*, 1189:60–73, 2009.

[104] H. Gallagher, G. Garvey, and G. P. Zeller. Neutrino-nucleus interactions. *Ann. Rev. Nucl. Part. Sci.*, 61:355–378, 2011.

[105] G. T. Garvey, D. A. Harris, H. A. Tanaka, Rex L. Tayloe, and G. P. Zeller. Recent advances and open questions in neutrino-induced quasi-elastic scattering and single photon production. *Phys. Rept.*, 580:1–45, 2015.

[106] L. Alvarez-Ruso, Y. Hayato, and J. M. Nieves. Progress and open questions in the physics of neutrino cross sections at intermediate energies. *New J. Phys.*, 16:075015, 2014.

[107] T. Katori and M. Martini. Neutrino–nucleus cross sections for oscillation experiments. *J. Phys.*, G 45(1):013001, 2018.

[108] M. Betancourt et al. Comparisons and challenges of modern neutrino scattering experiments (TENSIONS2016 Report). *Phys. Rept.*, 773-774:1–28, 2018.

[109] A. Bodek and T. Cai. Removal energies and final state interaction in lepton nucleus scattering. *Eur. Phys. J.*, C 79(4):293, 2019.

[110] R. R. Whitney, I. Sick, J. R. Ficenec, Robert D. Kephart, and W. P. Trower. Quasielastic electron scattering. *Phys. Rev.*, C 9:2230–2235, 1974.

[111] P. D. Zimmerman and M. R. Yearian. Fermi momenta and separation energies obtained from the quasi-elastic scattering of electrons from ^{48}Ca and ^{40}Ca. *Z. Phys.*, A 278(3):291–293, Sep 1976.

[112] E. J. Moniz, I. Sick, R. R. Whitney, J. R. Ficenec, Robert D. Kephart, and W. P. Trower. Nuclear fermi momenta from quasielastic electron scattering. *Phys. Rev. Lett.*, 26:445–448, 1971.

[113] M. Tanabashi et al. Review of particle physics. *Phys. Rev.*, D 98(3):030001, 2018.

[114] D. H. Perkins. Neutrino interactions. In J. D. Jackson and A. Roberts, editors, *Proceedings of the 16th International Conference on High-Energy Physics, 'ICHEP 72', Batavia, Illinois, September 6–13, 1972*, volume 4, pages 189–247, Batavia, 1973. National Accelerator Laboratory Publications Office.

[115] W. A. Mann et al. Study of the reaction $\nu + n \to \mu^- + p$. Reported at 'ICHEP 72' (paper #784); the data are published in Ref. [114], 1972.

[116] S. J. Barish et al. An inclusive look at νp and νn charged-current reactions below 6 GeV. Technical Report COO-1428-428, ANL-HEP-CP-75-38, Argonne National Laboratory, 1976.

[117] R. A. Singer. Study of the reaction $\nu + n \to \mu^- + p$. In M. A. Markov, G. V. Domogatsky, A. A. Komar, and A. N. Tavkhelidze, editors, *Proceedings of the International Conference on Neutrino Physics and Astrophysics (Neutrino'1977), Baksan Valley, USSR, June 18–24, 1977*, volume 2, pages 95–104, Moscow, 1978. "Nauka".

[118] L. A. Ahrens et al. A new limit on the strength of mixing between ν_μ and ν_e. *Phys. Rev.*, D 31(11):2732–2736, 1985.

[119] K. Furuno et al. BNL 7-foot bubble chamber experiment: Neutrino deuterium interactions. KEK preprint 2003-48, RCNS-03-01; reported at the 2nd International Workshop on Neutrino-Nucleus Interactions in the Few GeV Region 'NuInt 2002', Irvine, California, USA, December 12–15, 2002. The paper presents a reanalysis of the data from Ref. [25].

[120] N. Suwonjandee. *The measurement of the quasi-elastic neutrino-nucleon scattering cross section at the Tevatron.* PhD thesis, Cincinnati University, 2004.

[121] L. B. Auerbach et al. Measurements of charged current reactions of ν_μ on ^{12}C. *Phys. Rev.*, C 66:015501, 2002.

[122] M. M. Block et al. Neutrino interactions in the CERN heavy liquid bubble chamber. *Phys. Lett.*, 12(3):281–285, 1964.

[123] T. Eichten et al. Measurement of the neutrino-nucleon and antineutrino-nucleon total cross-sections. *Phys. Lett.*, B 46:274–280, 1973.

[124] M. Haguenauer. Gargamelle experiment. In J. R. Smith, editor, *Proceedings of the 17th International Conference on High Energy Physics, London, England, UK, July 1–10, 1974*, pages IV–9, Didcot, Berkshire, UK, 1975. Rutherford High Energy Laboratory.

[125] M. Rollier. Elastic neutrino and anti-neutrino interactions. In *Proceedings of the International Colloquium on High Energy Neutrino Physics, Paris, France, March 18–20, 1975*, pages 349–355, Paris, 1975. Éditions du Centre National de la Recherche Scientifique.

[126] P. Musset and J. P. Vialle. Neutrino physics with Gargamelle. *Phys. Rept.*, 39:1–130, 1978.

[127] S. K. Singh and E. Oset. Quasielastic neutrino (anti-neutrino) reactions in nuclei and the axial vector form-factor of the nucleon. *Nucl. Phys.*, A 542:587–615, 1992.

[128] A. M. de la Ossa Romero. *Study of accelerator neutrino interactions in a liquid argon TPC*. PhD thesis, Granada University & CAFPE, Granada, 2007.

[129] H. J. Grabosch et al. Investigation of quasielastic neutrino and anti-neutrino reactions in the energy range below 20 GeV. Technical Report PHE-86-11, Institute of High-Energy Physics, Zeuthen, 1986.

[130] J. Wolcott et al. Measurement of electron neutrino quasielastic and quasielasticlike scattering on hydrocarbon at $\langle E_\nu \rangle = 3.6$ GeV. *Phys. Rev. Lett.*, 116:081802, 2016.

[131] M. Betancourt et al. Direct measurement of nuclear dependence of charged current quasielasticlike neutrino interactions using MINERνA. *Phys. Rev. Lett.*, 119:082001, 2017.

[132] C. E. Patrick et al. Measurement of the muon antineutrino double-differential cross section for quasielastic-like scattering on hydrocarbon at $E_\nu \sim 3.5$ GeV. *Phys. Rev.*, D 97:052002, 2018.

[133] X. G. Lu et al. Measurement of final-state correlations in neutrino muon-proton mesonless production on hydrocarbon at $\langle E_\nu \rangle = 3$ GeV. *Phys. Rev. Lett.*, 121(2):022504, 2018.

[134] A. A. Aguilar-Arevalo et al. First measurement of monoenergetic muon neutrino charged current interactions. *Phys. Rev. Lett.*, 120:141802, 2018.

[135] K. Abe et al. First measurement of the ν_μ charged-current cross section on a water target without pions in the final state. *Phys. Rev.*, D 97:012001, 2018.

[136] F. James and M. Roos. MINUIT – a system for function minimization and analysis of the parameter errors and correlations. *Comput. Phys. Commun.*, 10(6):343–367, 1975.

[137] F. James. *MINUIT – function minimization and error analysis: Reference manual version 94.1*, 1994. CERN-D-506.

[138] A. Bodek and J. L. Ritchie. Fermi motion effects in deep inelastic lepton scattering from nuclear targets. *Phys. Rev.*, D 23(5):1070–1091, 1981.

[139] D. Ruterbories et al. Measurement of Quasielastic-Like Neutrino Scattering at $\langle E_\nu \rangle \sim 3.5$ GeV on a hydrocarbon target. *Phys. Rev.*, D 99(1):012004, 2019.

[140] C. Andreopoulos et al. GENIE physics & user manual, version 3.0.0.xx. link to the instant release: https://genie-docdb.pp.rl.ac.uk/DocDB/0000/000002/003/man.pdf, 2019.

[141] L. M. Kerby, S. G. Mashnik, and A. J. Sierk. Comparison of expanded preequilibrium CEM model with CEM 03.03 and experimental data, 2014. arXiv:1401.4404 [nucl-th].

[142] S. G. Mashnik and L. M. Kerby. MCNP6 fragmentation of light nuclei at intermediate energies. *Nucl. Instrum. Meth.*, A 764:59–81, 2014.

[143] S. G. Mashnik, L. M. Kerby, K. K. Gudima, A. J. Sierk, J. S. Bull, and M. R. James. Production of energetic light fragments in extensions of the CEM and LAQGSM event generators of the Monte Carlo transport code MCNP6. *Phys. Rev.*, C 95(3):034613, 2017.

[144] R. A. Arndt, I. I. Strakovsky, and R. L. Workman. The SAID PWA program. *Int. J. Mod. Phys.*, A18:449–455, 2003.

[145] R. A. Arndt, W. J. Briscoe, I. I. Strakovsky, and R. L. Workman. Extended partial-wave analysis of πN scattering data. *Phys. Rev.*, C 74:045205, 2006.

[146] The SAID partial-wave analysis facility and full database are available at the website of George Washington University `http://gwdac.phys.gwu.edu`.

[147] L. L. Salcedo, E. Oset, M. J. Vicente-Vacas, and C. Garcia-Recio. Computer simulation of inclusive pion nuclear reactions. *Nucl. Phys.*, A 484:557–592, 1988.

[148] K. S. Kuzmin, V. V. Lyubushkin, and V. A. Naumov. Lepton polarization in neutrino nucleon interactions. *Mod. Phys. Lett.*, A 19:2815–2829, 2004.

[149] K. S. Kuzmin, V. V. Lyubushkin, and V. A. Naumov. Extended Rein-Sehgal model for tau lepton production. *Nucl. Phys. B (Proc. Suppl.)*, 139:158–161, 2005.

[150] Ch. Berger and L. M. Sehgal. Lepton mass effects in single pion production by neutrinos. *Phys. Rev.*, D 76:113004, 2007.

[151] H. S. Budd, A. Bodek, and J. Arrington. Vector and axial form-factors applied to neutrino quasielastic scattering. *Nucl. Phys. B (Proc. Suppl.)*, 139:90–95, 2005.

[152] T. Golan, J. T. Sobczyk, and J. Zmuda. NuWro: the Wroclaw Monte Carlo generator of neutrino interactions. *Nucl. Phys. B (Proc. Suppl.)*, 229-232:499–499, 2012.

[153] J. Nieves, I. Ruiz Simo, and M. J. Vicente Vacas. Inclusive charged-Current neutrino-nucleus reactions. *Phys. Rev.*, C 83:045501, 2011.

[154] K. Gallmeister, U. Mosel, and J. Weil. Neutrino-induced reactions on nuclei. *Phys. Rev.*, C 94:035502, 2016.

[155] S. Dolan, U. Mosel, K. Gallmeister, L. Pickering, and S. Bolognesi. Sensitivity of neutrino-nucleus interaction measurements to $2p2h$ excitations. *Phys. Rev.*, C 98(4):045502, 2018.

[156] J. M. Nieves, I. Ruiz Simo, and M. J. Vicente Vacas. The nucleon axial mass and the MiniBooNE quasielastic neutrino-nucleus scattering problem. *Phys. Lett.*, B 707:72–75, 2012.

[157] Y. Hayato. NEUT. *Nucl. Phys. B (Proc. Suppl.)*, 112:171–176, 2002.

[158] Y. Hayato. A neutrino interaction simulation program library NEUT. *Acta Phys. Polon.*, B 40:2477–2489, 2009.

[159] R. W. Peelle. "Peelle's Perinent Puzzle". Informal memorandum dated October 13, 1987, Oak Ridge National Laboratory, Oak Ridge, Tennessee, USA.